FACULDADE DE ENGENHARIA DA UNIVERSIDADE DO PORTO

Design of a propulsion system for an underwater benthic Lander

José Miguel Reis e Rego

Mestrado Integrado em Engenharia Mecânica

Supervisor: Mário Vaz

Second Supervisor: Filipe Gonçalves

February, 2021

Design of a propulsion system for an underwater benthic Lander

José Miguel Reis e Rego

Mestrado Integrado em Engenharia Mecânica

February, 2021

Resumo

Esta dissertação apresenta um projeto inicial de um sistema de propulsão para um lander subaquático produzido pelo INEGI.

A tese inicia-se com uma introdução acerca da relevância económica da exploração dos oceanos e uma explicação sucinta do contexto do projeto para o qual o lander foi desenvolvido.

É feita uma revisão dos tipos de veículos subaquáticos existentes atualmente, com foco especial nos landers e nas suas características. São apresentados os materiais utilizados em construções subaquáticas e é escolhido o material para desenvolver o projeto.

De seguida, são apresentados os conceitos do Método dos Elementos Finitos, no qual a análise do software utilizado se baseia.

O quarto capítulo foca-se na apresentação do lander produzido pelo INEGI e são apresentados o equipamento, material, planos futuros e cálculos relevantes para o projeto.

De seguida, é feita uma revisão acerca da mobiliade de veículos subaquáticos. É também realizada uma análise de cada solução apresentada e é escolhido o sistema de propulsão para o projeto.

No capítulo seguinte são propostas soluções para a conecção com o lander. Depois de uma análise de cada possibilidade, é escolhida uma proposta e é feito um modelo da mesma. É realizada uma análise estrutural, recorrendo ao software Ansys e são feitas iterações para ultrapassar as dificuldades apresentadas. Após obter um modelo satisfatório, é feita uma análise mais aprofundada das peças críticas.

Por fim, é feita uma análise modal e uma análise à encurvadura.

Palavras-chave: Análise estrutural, Sistema de propulsão, Lander subaquático, Método dos elementos initos, Poliacetal.

Abstract

This dissertation presents an initial project of a propulsion system for an underwater lander developed by INEGI.

The thesis starts with an introduction about the economic relevance of oceans' exploration and a succinct explanation of the context of the project for which the lander was developed.

A review on types of underwater vehicles is made, with special focus on landers, highlighting their purpose and main characteristics. The materials used in these solutions are presented and a choice is made regarding the material proposed for the project.

The basic concepts of the Finite Element Method, in which the software used in the projected is based, are presented.

The fourth chapter is focused on INEGI's benthic lander, where all the equipment, material, relevant calculations and future plans for the lander are presented.

Afterwards, a review on mobility in underwater vehicles is made. An analysis of each solution presented is held and the propulsion system for the project is chosen.

In the next chapter, initial connections to the lander are proposed. After an analysis of each one, a choice is made and a model is developed. Structural analyses are developed using Ansys software and iterations are made in order to overcome mechanical difficulties. After achieving a satisfactory model, a more in depth analysis to the critical pieces is developed.

Lastly, modal and buckling analysis are made.

Keywords: Structural analysis, Propulsion system, Underwater lander, Finite element method, Methylene Polyoxide.

Agradecimentos

Ao professor Mário Vaz, por ter aceitado o tema proposto e ter colaborado na sua elaboração.

Ao INEGI, em concreto aos engenheiros Tiago Morais e Filipe Gonçalves pelo tema proposto e pelo auxílio incansável demonstrado para o desenolvimento deste projeto.

Aos meus pais, mana, Tozé, família e ao Scott pelo apoio e disponibilidade.

Aos meus amigos, por todas as grandes ideias em que alinharam.

Contents

List of Figures

List of Tables

Nomenclature

V_l	Volume of the lander
ν	Poisson's ratio
ρ	Density
ρ_f	Fluid's density
B_f	Final buoyancy of the lander
B_i	Initial buoyancy of the lander
V_d	Volume of fluid displaced
W_f	Final weight of the lander
W_i	Initial weight of the lander
W_w	Wet weight
AMALIA	Algae-to-MArket-Lab IdeAs
AUV	Autonomous Underwater Vehicles
B	Buoyancy
C	Current
CFRP	Carbon Fiber Reinforced Plastics
DOF	Degrees of freedom
E	Young Modulus
EU	European Union
FEM	Finite Element Method
g	Gravitational acceleration
GDP	Gross Domestic Product
GFRP	Glass Fiber Reinforced Plastics
HROV	Hybrid Remotely Operated Vehicle

INEGI	Institute of Science and Innovation in Mechanical and Industrial Engineering
kg	Kilogram
LARS	Launch and Recovery System
m	Meter
min	Minute
Pa	Pascal
PVW	Principle of Virtual Work
ROV	Remotely Operated Vehicles
s	Second
T	Thrust
VBS	Variable buoyancy system
W	Weight
WOI	World Ocean Initiative

Chapter 1

Introduction

1.1 Ocean exploration

The ocean has a decisive role in the preservation and regulation of life on earth and particularly in human life. It contributes to the preservation and enrichment of biodiversity, is a home to natural resources, represents a way for transportation by boats, regulates weather and climate changes, can be explored as a source of energy, among many other possibilities [1]. All of these contribute to a great impact in global economy, making the ocean the world's seventh largest economy if put into Gross Domestic Product (GDP) terms [2]. The European Union (EU) Blue Economy report 2020 [3], built on the most recent processed data - corresponding to the year of 2018-, sets the relevance of the blue economy for Europe and its future, as can be seen in Table 1.1 . These values are expected to increase thanks to the Green Deal will help to boost the blue economy, namely on areas such as research, aquaculture, tourism, energy and ocean pollution [3].

Table 1.1: EU Blue Economy established sectors, 2018 [3].

Indicator	EU Blue Economy 2018
Gross value added	218 billion €
Gross profit	94 billion €
Employment	5 million people
Average annual salary	24700 €

In spite of this, the data relating to Portugal, as can be seen through Figures 1.1 and 1.2, reveals that a great percentage of the country's blue economy relies on tourism, an area highly affected by the pandemic of COVID-19. Thus, it is expected to shrink in 2020 and 2021. Nevertheless, Portugal possesses the sovereignty or jurisdiction of 41% of the marine space of the countries that belong to the European Union [4]. Thus, it represents a field with high potential of exploration and investment, regarding the european funds. InvestEU is one of these funds and, instead of purely stimulating the economic recovery like previous funds, its main purpose is to accelerate measures under the Green Deal [3]. It is thus, expected that the European Union straightens the investment support, once projections indicate that Blue Economy will have a crucial role in order to reach the goals set regarding biodiversity and greenhouse gas emissions.

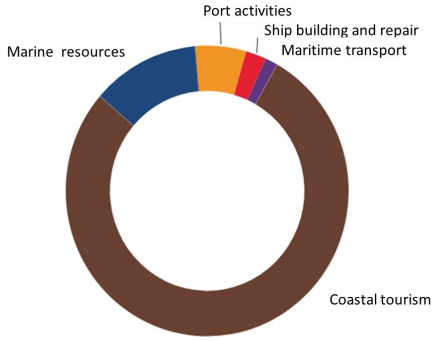

Figure 1.1: Distribution of value added at factor cost (GVA) by sector in Portugal, 2018 [5].

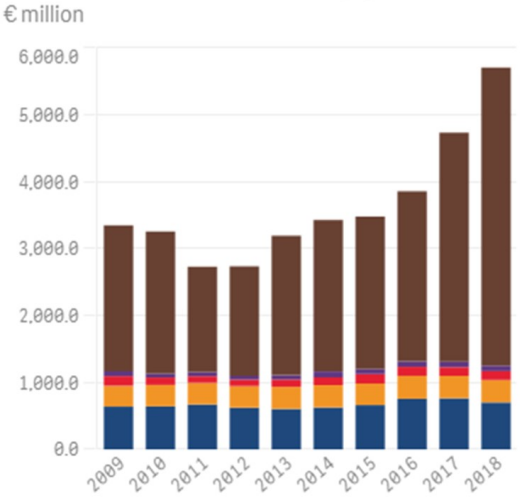

Figure 1.2: Value added at factors cost by sector in Portugal [5].

Mankind has demonstrated curiosity to explore the ocean and its bottom for a long time. It dates back to the eighth century when Vikings tried to measure the deepness of the ocean with a rope with weights attached. Since the nineteenth century, there has been an arise and development of new technologies that allowed to deepen the knowledge and exploration of the oceans. In 1818, Jonh Ross was able to catch worms and jellyfish at a depth of approximately 2000 meters, offering for the first time evidence of the existence of life in deep waters. In 1930, William Beebe and Otis Barton become the first humans to explore the deep sea. It was done in an unique spherical deep-sea submersible named "Bathysphere", which was unpowered and lowered into the ocean on a cable. In 2012, the movie director and deep sea enthusiast James Cameron completed the first solo dive to the Mariana trench, reaching the ocean's deepest point [6].

In spite of all these accomplishments, according to the National Ocean Service, 80% of the ocean has not been explored, mapped nor even observed [7]. Thus, the ocean exploration is and will be in years to come an important sector for many governments, institutions and companies.

1.2 The AMALIA project

Algae-to-MArket-Lab IdeAs (AMALIA) is the name of the project being developed in Institute of Science and Innovation in Mechanical and Industrial Engineering (INEGI) in association with other high education institutions and companies. In the northwest of the Iberian Peninsula was registered an unusual growth of an algae, an invasive species that threatens the native species. This contributed to a negative impact on biodiversity, degradation of important biotipes that can lead to an indirect negative impact on food provision, aqua-culture and fisheries, water storage and provision and recreation and tourism, among others [8]. All of these contribute to indirect and negative economic and social impact.

Although, for now, still being an unexploited biological resource, macro algae is seen as a potential resource for many industries, namely: cosmetic, food and feed, pharmaceutical and even energy. This is due to its attractive characteristics such as quick growth, adaptability to most climate zones and high content of valuable carbohydrates, proteins and lipids [9]. Having this in mind, the AMALIA project aims to turn this undesired situation into an opportunity, exploiting the potential properties of these seaweeds. In order to achieve this goal, INEGI has developed a modular benthic lander to collect data about the growth of these species and further comprehend its characteristics. In order to cover more areas in a single deployment, a propulsion system for the lander must be developed.

Chapter 2

Underwater vehicles

Ocean exploration has evolved drastically in recent years thanks to the development of marine technologies accompanying the growth of blue economy. In fact, recently, in October 2019, in a conference organized by World Ocean Initiative (WOI) about the transformation to the blue economy, 370 pledges were made totalling almost US$ 64 bn [10].

The use of unmanned vehicles has allowed to explore places with extreme conditions or inaccessible by humans, as well as perform tasks that previously required human labour. Among the types of underwater vehicles, presented in Figure 2.1, there are four main kinds of unmanned robots used for ocean exploration: Remotely Operated Vehicles (ROVs) , Autonomous Underwater Vehicles (AUVs) , hybrids and landers, that are presented in the next sections, as well as specific examples of vehicles used to explore the ocean.

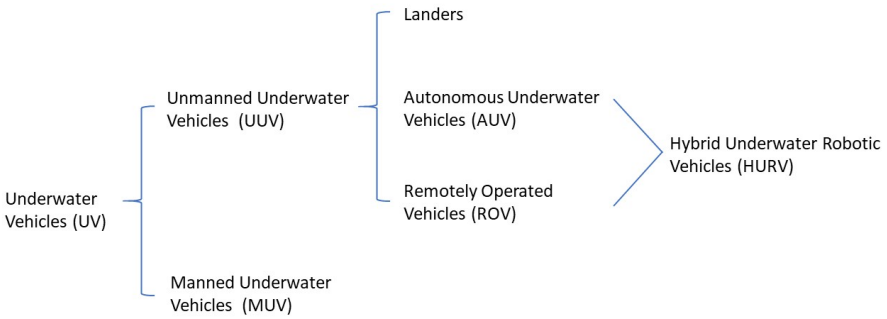

Figure 2.1: Different kinds of underwater vehicles.

2.1 ROVs

ROVs are underwater highly maneuverable vehicles that are equipped with a cable that allows remote operation.

ROVs can be deployed until the desired depth through a launch and recovery system (LARS) such as a clump weight or a cage. This allows to use two different types of cables: one load carrying umbilical that connects the cage or weight to the vessel and a neutrally buoyant tether that connects the LARS to the ROV. Using this technique allows to protect the ROV until the operation depth. Furthermore, it does not require a variable buoyancy system for the ROV [11].

ROVs can also be directly deployed by hand for small vehicles, or by using cranes for bigger vehicles. The ROVs that are deployed using these techniques are usually used at low depths or, once in the water, descend to the desired depth through their propulsion or variable buoyancy systems [11].

In both deployment techniques, the tether is responsible for carrying electrical power, video and data signals, which allows for real time images, data analysis and also guarantees the ROV's independence of batteries. This allows the ROV to be underwater for a long period of time, even though it still relies on a source of energy on the surface.

The use of a tether presents downsides such as the possibility of getting tangled in rocks, fishing nets, fauna and other elements, as well as presenting a physical limitation to the vehicle operation.

Among these vehicles' utilities, the most common are exploration at high pressures or risky places for human lives and installation, inspection and maintenance of underwater structures such as ships, oil and gas structures and underwater pipelines. They can also be used to help in surveillance and security of ports, collect artifacts and recover underwater objects. An example of the usage of these vehicles in dangerous situations is the recovery of an atomic bomb that was lost in an aircraft accident in 1966 and was later recovered by the USA military [12, 13].

All over the world, there are numerous companies that focus on the development and production of ROVs, such as HPRROV, OCEANEERING or Delta Sub Sea Deep Ocean. Start-ups such as BlueRobotics and Chasing are setting a trend to develop low cost ROVs and components, allowing and encouraging the general public to explore the oceans.

ROV's size and weight varies highly with the requirements of the tasks aimed to perform. For demanding missions, they can be bigger than a car, while for recreational activities can be as small as a shoes box. In Table 2.1 are listed different types of ROVs as well as their characteristics and two of them are presented in Figures 2.2 and 2.3.

Table 2.1: Data about 4 ROVs [16, 14, 17, 18].

Name	Max depth(m)	Max speed (m/s)	Dimensions (m)	Weight (kg)	Thrusters	Type	Notes
BlueROV2	100	1,5	0,457 x 0,338 x 0,254	10	6	Eletric	Low cost
CIDESI	2000	1,25	1,4 x 1,2 x 0,9	350	6	Eletric	Hyrdaulic manipulator
HERCULES	4000	0,77	3,9 x 2,2 x 1,9	2500	6	Hydraulic	
KIEL6000	6000	5,5	3,5 x 2,4 x 1,9	3500	7	Eletric	2 hydraulic manipulators

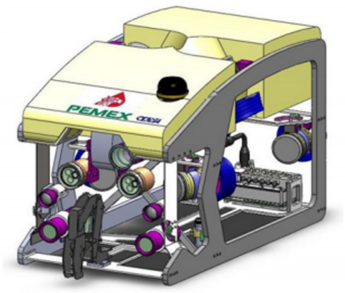

Figure 2.2: Model of CIDESI ROV [14].

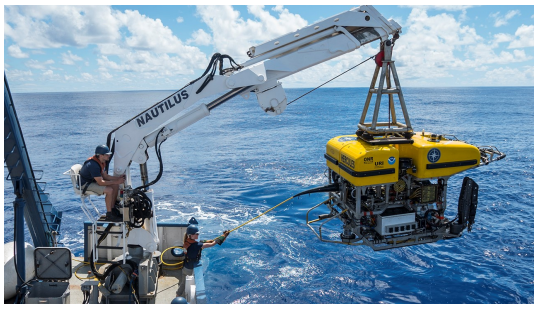

Figure 2.3: Hercules ROV [15].

2.2 AUVs

AUVs are unmanned, autonomous selfpropelled underwater vehicles. They are usually deployed from a surface vessel and their working time may vary from a few hours to several days, depending on the kind of work and their power supplies. The depth of work may be as deep as 6000 m and they generally circulate at a speed up to 1.5-2 m/s. In spite of the need of a vessel, being an autonomous vehicle, its operation is independent of the distance to the boat. The use of AUVs is a way of complementing the research work done by research teams in vessels [19, 20]. There are many areas in which AUVs enrol, but the most common are research, commercial applications and surveillance applications [19].

Contrarily to ROVs, AUVs must be preprogrammed to follow a defined course. In order to reduce drag effects, AUVs are usually torpedo shaped, but can have complex geometries as well, depending on the type of job performed and the devices required to do so.

AUVs have the capacity to maintain a direct trajectory through the water, because generally are not propelled using a buoyancy engine, which would cause the vehicle to have an undulating trajectory. This represents a convenience for geoscience applications that require constant altitude [19]. One of the advantages of AUVs also represents a big challenge: continuously collecting large volumes of data demands more storage capacity and data analysis [21].

Numerous factors need to be taken into account before the deployment and of programming the AUV. It should not be deployed in areas with military, shipping or fishing activities because of the possibility of acoustic interference, collision risk and net entanglement. Besides, currents must be taken into account, once they can affect the speed and stability of the vehicle and consequently the reliability of the data collected [19, 22].

Besides shape and geometry, AUVs are characterized by maximum operation depth, maximum speed and its communication and navigation systems. In Table 2.2 data of models of AUVs is listed and two of them are presented in Figures 2.4 and 2.5.

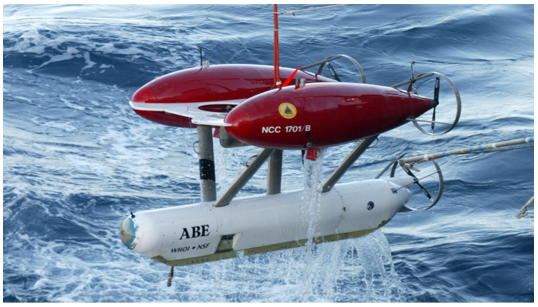

Figure 2.4: ABE AUV [23].

Figure 2.5: DEPTHX AUV [24].

Table 2.2: Specific data about 3 AUVs [25].

Name	Max depth (m)	Max speed (m/s)	Dimensions (m)	Weight (kg)	Propulsion	Type
ABE	4500	0.77	3 x 2 x 2.5	550	5 thrusters	Electric
DEPTHX	1000	No data	4.26 x 3.04 x 3.04	1300	6 thrusters	Electric and hydraulic
HAUV	60	0.5	0.107 x 0.100 x 0.041	79	5 thrusters	Electric

2.3 Hybrid vehicles

Hybrid vehicles, also known as hybrid ROVs (HROVs) present the advantages of both ROVs and AUVs, meaning that they can operate in both ways, either remotely by an operator or autonomously. They are usually used as an AUV for operations in broad areas and as an ROV for close-up interventions, that are more complex and thus must be performed by an operator. Most hybrid vehicles can switch between these two modes during a single cruise deployment, making deep-sea exploring more cost effective [26].

In the Table 2.3 are presented specifications about three hybrid vehicles and two of them are presented in Figures 2.6 and 2.7.

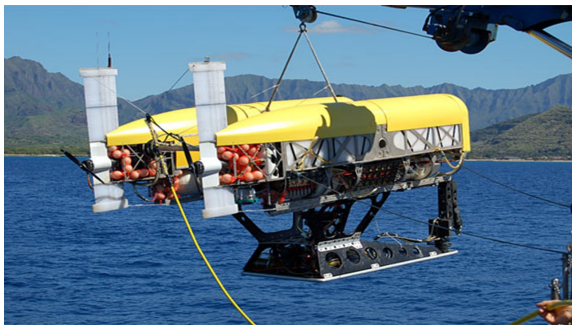

Figure 2.6: Nereus hybrid vehicle [27].

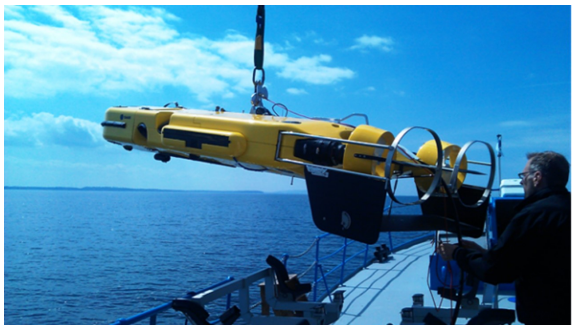

Figure 2.7: SAROV hybrid vehicle [28].

Table 2.3: Specific data about three hybrid vehicles [25, 29, 30, 31].

Name	Max depth (m)	Max speed (m/s)	Dimensions (m)	Weight (kg)	Propulsion	Type
Nereus	110000	2.5	3.1 x 2.3 x 4.7	2800	5 x 1 kW thrusters	Electric and hydraulic
SAROV	300	3	3 x 1,3 x 0,8	730	2500 N - thurst force	Electric
Fusion	300	No data	0,686 x 0,275 x 0,508	27.5	7 electric thrusters	Electric

2.4 Landers

Lander is a general term for unmanned underwater vehicles that operate at the ocean floor. They usually are installed using the free fall method, until they reach the sea floor and operate independently from there. However, in order to avoid a collision with the seafloor when dropped, which can be harmful to the lander, they can also be deployed close to the ocean floor, through a hoist. This also allows to deploy the vehicle in a specific position, but requires manpower and is therefore a more expensive alternative. Besides, it is not a suitable option for lower depths.

Once the landers reach the seafloor, they stand static, so they are usually used for long time data acquisition in the same area [32]. In order to achieve this, the structure can be composed by a set of sensors, a data storage system, batteries, cameras, equipment for *in situ* experiments and sometimes baits to attract fauna.

Landers are usually equipped with ballast weights in order to have negative buoyancy and thus free fall to the sea floor. Once the time required to complete the operation has passed, they are released by an acoustic command or a timer. After detaching this mass, the lander gets positive buoyancy and goes up to the surface. It is then collected and the gathered data is analysed [32, 33].

These vehicles are used, among many other possibilities, to study sea floor constitution, microseismic activity, deep-sea fauna and flora and long term measurements of near bottom currents and tides [32].

The main advantages of using these vehicles are low disturbance, ease of use, capability of long-time implementation, little demanding of ship time and the possibility to carry experiments and measurements *in situ* [32].

In the table 2.4, are listed three landers and their main characteristics. In the dimension column are presented respectively the height and the diameter of the circumference that circumscribes the projected area of the lander. For INEGI's lander the dimensions presented are just for reference, once the lander is an adjustable tripod and can present numerous set-ups.

Table 2.4: Specific data about three landers [34, 35].

Company/Institute	Maximum depth (m)	Dimensions (m)	Maximum operation time	Equipment
Oregon Marine Research	20	0,06 x 0,043	20 min	3 cameras, baits.
Shenyang Institute of Automation	7000	2,3 x 3	30 days	Funnerl trap, cameras, sampler, LEDs, CTD profiler, dissolved oxigen sensor.
INEGI	200	1,854 x 3,175	30 days	Spectral camera, light sources.

2.5 Types of landers according to deepness

Landers can be classified according to the depth in which they operate. Shallow water landers operate in depths up to 500 m. At this range of deepness, the hydrostatic pressure is reduced when compared to greater depths and the loads associated with waves and currents decrease significantly with deepness.

Mid-water landers can operate as deep as 2500 m. At this depth, the hydrostatic pressure values are more considerable, while the load caused by currents is negligible. Deep waters landers function at more profound depths, but the kinds of loads that must be considered do not differ from mid-water landers. However, the magnitude of the hydrostatic increases substantially [36].

2.6 Types of landers according to geometry

Landers may be categorized according to their geometry and size. Macro open-frame landers are designed in order to allow the flow of water through the structure, so that they are not affected by currents. In what comes to geometry, these are similar to macro open-frame landers. The main difference between them is that macro open-frame landers are designed for long term missions and usually there is more equipment required and consequently the size of the lander increases. Flat shape landers use a structure that makes the currents generate a downwards force, anchoring the lander when the tides are more powerful. In Figures 2.8 to 2.10 are presented examples of the categories mentioned.

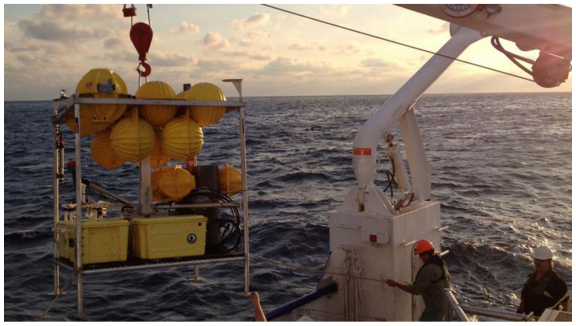

Figure 2.8: Macro open frame lander [37].

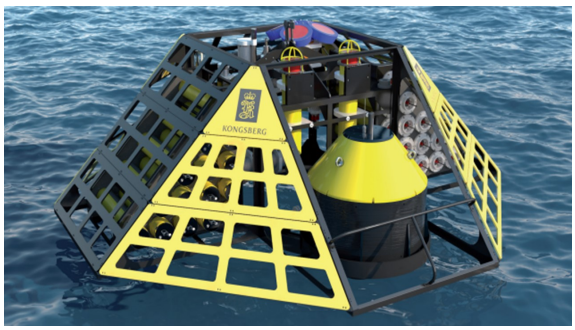

Figure 2.9: Flat shape lander [38].

Figure 2.10: Micro open frame lander [39].

2.7 Materials used in underwater solutions

In the design of mechanical parts, the choice of the materials is one of the most important steps. The choice cannot only be based on the stresses and deflections, but must also take into consideration the cost, environmental impact, temperature and corrosion to which it will be exposed, among many other aspects. It is therefore important to study materials used in underwater solutions and their properties.

In this chapter are presented materials suitable for structural underwater use and explained their advantages and disadvantages. In the end of the chapter is chosen the material used for the project.

2.7.1 Ocean environment

The ocean presents a rough environment for materials. The currents, fauna, the salinity of the water, the hydrostatic pressure and mainly the corrosive effect of sea water affect their performance and thus, the choice in the project. It is crucial to secure the reliability of the vehicles. Due to their relatively high costs, it is important to make sure that these withstand the rough conditions and can be used in several missions.

2.7.2 Lander's requirements

The main requirements of a lander are to withstand ocean's environment and the loads acting on it: the hydrostatic pressure, currents' forces and other loads related to the equipment that operates in the lander. Furthermore, it is desirable to make landers as lightweight as possible, without compromising its structural behaviour. This way, the landers are easier to handle and require less equipment with positive buoyancy, which usually is associated with a high cost, due to the use of expensive foams or glass spheres.

2.7.3 Aluminium

Aluminium is a widely used material in underwater vehicles, since it is inexpensive and lightweight. However it presents low strength compared to other materials, as can be seen in Table 2.5. Besides, the welding process is dangerous and must be set under strict conditions, which can lead to problems in the production of the equipment [32, 40].

In what comes to corrosion, aluminium presents acceptable results. However, depending on the series of the aluminium used, it may be necessary to do surface treatments, such as anodizing, electrolysis nickel plating, electroless nickel plating or painting [41].

2.7.4 Stainless steel

Stainless steels are alloys of iron with nickel, chromium and often more elements. This kind of material can also be an option, once it presents excellent corrosion resistance, namely to salt water. Stainless steel present better mechanical properties than aluminium, such as the Young's modulus that is the highest of the materials presented. It presents, however, a much higher density, that can affect the requirements mentioned for the lander [32, 40].

2.7.5 Titanium

Even though titanium is one of the most abundant metals in earth's crust, the process of extracting the metal from the oxide is extremely difficult, which makes it much more expensive than most materials presented. However, it also has excellent mechanical properties, namely great durability in salt water, and even inferior density than stainless steel. It also presents low thermal conductivity and low expansion coefficients, which can be relevant in underwater environments [40]. Furthermore, the welding requires a strictly controlled atmosphere as well as specialised welding equipment, contributing to high costs of production. Another disadvantage is that polishing titanium is a risky task, once its dust can ignite spontaneously [32]. Titanium alloys present generally better mechanical properties, however, the cost can be double of pure titanium and 10 times more than aluminium [40].

2.7.6 Composites

Composites with high stiffness and strength are usually constituted of continuous fibers embedded in a thermosetting resin. The matrix material provides ductility and toughness and transmits the loads to the fibers. This also means that the matrix protects the fibers from damage caused by handling or the environment. However, it is also the matrix that limits the service temperature and processing conditions.

Both Carbon Fiber Reinforced Plastics (CFRP) and Glass Fiber Reinforced Plastics (GFRP) are examples of widely used composites, with great mechanical properties and low density. However, CFRPs present overall better properties and that is reflected on the price. A negative point

regarding these composites is that individual fibers are prone to buckling and shearing failures [40].

2.7.7 Polymers

Polymeric materials are another option for underwater vehicles. These materials usually present high resistance to corrosion, low density and price. Although they present low strength and worse mechanical properties than the materials presented before, their density is very appealing, once it contributes to the desirable high buoyancy of the vehicles, allowing to reduce costs.

2.7.7.1 Polyoxymethylene (POM or Acetal)

This polymer in particular is presented because of the suitable properties for the project and because it is the one used in the AMALIA lander.

Polyoxymethylene is a polymer commercially known as POM or Acetal. Its repeating unit is -(CH2O)n and the resulting molecule is linear and highly crystalline. Thanks to this, POM presents good fatigue resistance and stiffness and is easily moldable.

Its low density presents an advantage to its use in underwater solutions, besides the low price and the excellent resistance to salt water corrosion. It also presents natural lubricity and that is the reason why it is also used in mechanical applications, such as gears. However, this does not present any advantage for underwater use.

Blow molding, injection molding and sheet molding are the main processes that can be used for the production of POM products. However, due to the shrinkage on cooling, the wall thickness must be at least of 0.1mm. Additive manufacturing, also known as 3D printing, is also an option to manufacture POM. However, the final product is less homogeneous and thus may not present mechanical properties as good as when done by molding. Machining is another option and can be considered the best one for production of small numbers of small series, as should be the case of the project.

Table 2.5 presents the properties of the materials mentioned.

Table 2.5: Properties of materials used in underwater vehicles [40].

Material	Density(kg/m^3)	E(GPa)	Yield strength(MPa)	Compressive strength (MPa)	Price (€/kg)	Corrosion Resistance
Aluminium	2650-2770	69-76	118-263	109-251	2,03-2,19	Acceptable
Stainless steel	7610-7870	190-210	257-1140	252-1200	2,59-2,78	Excellent
Pure titanium	4510	100-105	277-359	180-210	10,9-12,5	Excellent
Titanium alloys	4430-4790	110-120	701-1090	680-1150	19,4-21	Excellent
Epoxi with CFR	1500-1600	69-150	550-1050	440-840	29,7-32,9	Excellent
Epoxi with GFR	1750-1970	15-28	207-304	207-257	30,2-33,2	Excellent
POM	1390-1430	2,6-3,2	57,2-71,7	105-116	2,39-2,51	Excellent

2.7.8 Material choice

After an analysis of the relevant properties of the materials presented, a table was built rating each of the materials from 1 to 5, in which 1 corresponds to "not satisfying at all" and 5 means "very satisfying".

Table 2.6: Table of decision for the material

Material	Corrosion resistance	Mechanical properties	Density	Price	Average
Aluminium	4	4	3	5	4
Stainless Steel	5	4	1	5	3,75
Titanium/Titanium alloys	5	5	2	2	3,5
CFRP/GFRP	5	5	4	1	3,75
POM	5	3	5	5	4,5

The elaboration of Table 2.6 allows to choose objectively POM for the project in consideration. From the company's point of view, this decision can be even more valued, taking in account the experience handling this material.

Chapter 3

Finite Element Method for 3D solids

Finite Element Method (FEM) is a numerical method used to solve mechanics problems governed by a set of partial differential equations. The domain of the problem is first discretized into small elements, in which the profile of the displacements is assumed in simple forms in order to obtain element equations. These are then assembled together with adjoining elements to create the global finite element equation for the whole domain of the problem considered. Equations created for the global problem domain can be solved for the entire displacement field [42].

This method was used for the analysis of the structure developed in the project, for structural, buckling and modal analysis. This was done recurring to the AnsysR©Academic Research Mechanical, Release 20.2 license , since it is provided by FEUP and the one used in INEGI.

Next, are presented the basis of the FEM, in which the software is based.

3.1 Introductory theory

Let us consider a global coordinate system x, y and z and the 3D solid shown in Figure 3.1.

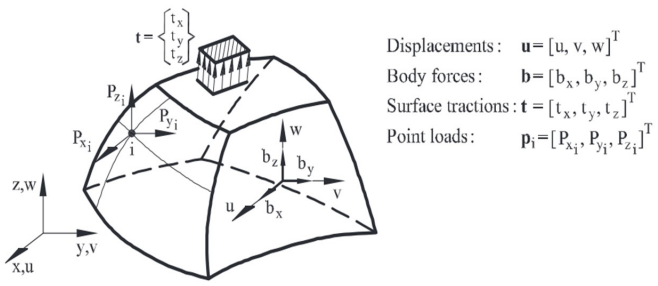

Figure 3.1: Generic 3D solid [42].

The displacement vector **u** of a considered point of the element has three components

$$\mathbf{u} = [u, v, w]^T \tag{3.1}$$

in which u, v, w are the displacements of the point in the directions of the axes x, y, z respectively.

In addition, the stress field of a 3D solid is defined by the six stress components

$$\sigma = [\sigma_x, \sigma_y, \sigma_z, \tau_{xy}, \tau_{xz}, \tau_{yz}]^T \tag{3.2}$$

in which $\sigma_x, \sigma_y, \sigma_z$ are normal stresses and $\tau_{xy}, \tau_{xz}, \tau_{yz}$ are tangential stresses.

The strain field of a 3D solid is defined by the six strain component of 3D elasticity and thus the vector is written as

$$\varepsilon = [\varepsilon_x \varepsilon_y \varepsilon_z \gamma_{xy} \gamma_{xz} \gamma_{yz}]^T \tag{3.3}$$

and

$$\varepsilon_x = \frac{\partial u}{\partial x} \qquad \varepsilon_y = \frac{\partial v}{\partial y} \qquad \varepsilon_z = \frac{\partial w}{\partial z}$$
$$\gamma_{xy} = \frac{\partial u}{\partial y} + \frac{\partial v}{\partial x} \qquad \gamma_{xz} = \frac{\partial u}{\partial z} + \frac{\partial w}{\partial x} \qquad \gamma_{yz} = \frac{\partial v}{\partial z} + \frac{\partial w}{\partial y}$$

where $\varepsilon_x, \varepsilon_y, \varepsilon_z$ are the normal strains and $\gamma_{xy}, \gamma_{xz}, \gamma_{yz}$ are the tangential strains.

Considering an isotropic material, it is possible to establish the relationship between the stress and the strain fields. For this, are only required the material properties E and ν that represent respectively the Young modulus and Poisson's ratio [42]:

$$\sigma = D(\varepsilon - \varepsilon^0) + \sigma^0 \tag{3.4}$$

where

$$D = \frac{E(1-\nu)}{(1+\nu)(1-2\nu)} \begin{bmatrix} 1 & \frac{\nu}{1-\nu} & \frac{\nu}{1-\nu} & 0 & 0 & 0 \\ & 1 & \frac{\nu}{1-\nu} & 0 & 0 & 0 \\ & & 1 & 0 & 0 & 0 \\ & & & \frac{1-2\nu}{2(1-\nu)} & 0 & 0 \\ Symmetrical & & & & \frac{1-2\nu}{2(1-\nu)} & 0 \\ & & & & & \frac{1-2\nu}{2(1-\nu)} \end{bmatrix} \tag{3.5}$$

At last, is also important to considerate the Principle of Virtual Work (PVW) for 3D solids, that is defined by [42]

$$\int\int\int_V \delta\varepsilon^T \sigma dV = \int\int\int_V \delta \mathbf{u}^T b dV + \int\int_A \delta \mathbf{u}^T t dA + \sum_i \delta a_i^T p_i \tag{3.6}$$

u in which V and A are respectively the volume and the surface of the solid over which the surface tractions $t = [t_x, t_y, t_z]^T$ and the body forces $b = [b_x, b_y, b_z]^T$ act and $p_i = [P_{x_i}, P_{y_i}, P_{z_i}]^T$ are the point loads acting in node i, while δa_i^T represents the virtual nodal displacements.

It is required C^0 continuity for the finite element approximation, once the integrals involve first derivatives of the displacement.

3.2 FEM - the four noded tetrahedron

The four-noded tetrahedron is a 3D element and a natural extension of the 3-noded triangle. It has 4 nodes and each presents three degrees of freedom (DOF) , accounting for a total of 12 DOFs for the element.

Let us consider a 3D body divided into four-noded tetrahedral elements, as the one represented in Figure 3.2.

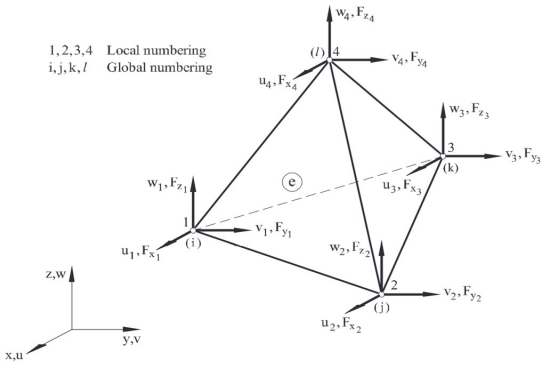

Figure 3.2: Four noded tetrahedron [42].

The displacement field in each element can be interpolated as

$$u = \begin{Bmatrix} u \\ v \\ w \end{Bmatrix} = \begin{Bmatrix} N_1u_1 + N_2u_2 + N_3u_3 + N_4u_4 \\ N_1v_1 + N_2v_2 + N_3v_3 + N_4v_4 \\ N_1w_1 + N_2w_2 + N_3w_3 + N_4w_4 \end{Bmatrix} = \sum_{i=1}^{4} N_i a_i^{(e)} = N a^{(e)} \tag{3.7}$$

where

$$N = [N_1, N_2, N_3, N_4] \quad ; \quad N_i = \begin{bmatrix} N_i & 0 & 0 \\ 0 & N_i & 0 \\ 0 & 0 & N_i \end{bmatrix} \tag{3.8}$$

and

$$a^{(e)} = \begin{Bmatrix} a_1^{(e)} \\ a_2^{(e)} \\ a_3^{(e)} \\ a_4^{(e)} \end{Bmatrix} \quad ; \quad a_i^{(e)} = \begin{Bmatrix} u_i \\ v_i \\ w_i \end{Bmatrix} \tag{3.9}$$

represent respectively the shape function matrix and the displacement vector for the element considered and the node i, respectively. The same interpolation has been used for all the displacements. Hence, the shape functions used are the same.

The four nodes of the element define a linear displacement field in 3D. Since it was assumed the same interpolations for the three components, it is sufficient to determine the shape functions of only one of them. In order to get the analytical form of the shape functions N_i, and choosing the displacement u, it is possible to write

$$u = \alpha_1 + \alpha_2 x + \alpha_3 y + \alpha_4 z \tag{3.10}$$

and the coefficients α_i can be obtained by substituting the nodal coordinates into Equation 3.10 and making the displacements equal to their nodal values:

$$\begin{aligned} u_1 &= \alpha_1 + \alpha_2 x_1 + \alpha_3 y_1 + \alpha_4 z_1 \\ u_2 &= \alpha_1 + \alpha_2 x_2 + \alpha_3 y_2 + \alpha_4 z_2 \\ u_3 &= \alpha_1 + \alpha_2 x_3 + \alpha_3 y_3 + \alpha_4 z_3 \\ u_4 &= \alpha_1 + \alpha_2 x_4 + \alpha_3 y_4 + \alpha_4 z_4 \end{aligned}$$

Through this system of equations, it is possible to solve for $\alpha_1, \alpha_2, \alpha_3$ and α_4. Substituting these results in Equation 3.10 and after rearranging the terms [42],

$$u = \sum_{i=1}^{4} \frac{1}{6V^{(e)}} (a_i + b_i x + c_i y + d_i z) u_i \tag{3.11}$$

The nodal shape function N_i is obtained by comparing Equations 3.11 and 3.7 as [42]:

$$N_i = \frac{1}{6V^{(e)}} (a_i + b_i x + c_i y + d_i z) \tag{3.12}$$

where $V^{(e)}$ represents the volume of the elementand the coefficients a_i, b_i, c_i and d_i can be obtained through

$$\begin{aligned} a_i &= det \begin{vmatrix} x_j & y_j & z_j \\ x_k & y_k & k \\ x_l & y_l & z_l \end{vmatrix} \quad ; \quad b_i = det \begin{vmatrix} x_j & y_j & z_j \\ x_k & y_k & z_k \\ x_l & y_l & z_l \end{vmatrix} \\ c_i &= det \begin{vmatrix} x_j & y_j & z_j \\ x_k & y_k & z_k \\ x_l & y_l & z_l \end{vmatrix} \quad ; \quad d_i = det \begin{vmatrix} x_j & y_j & z_j \\ x_k & y_k & z_k \\ x_l & y_l & z_l \end{vmatrix} \end{aligned} \tag{3.13}$$

and parameters for $i = 1,2,3,4$ are obtained by adequate cyclic permutation of the indexes i, j, k, l [42].

3.2.1 Strain matrix

Substituting 3.7 into 3.3, gives for a 3D elements with n=4 nodes:

$$\varepsilon = \sum_{i=1}^{4} \begin{Bmatrix} \frac{\partial N_i}{\partial x} u_i \\ \frac{\partial N_i}{\partial y} v_i \\ \frac{\partial N_i}{\partial z} w_i \\ \frac{\partial N_i}{\partial y} u_i + \frac{\partial N_i}{\partial x} v_i \\ \frac{\partial N_i}{\partial z} u_i + \frac{\partial N_i}{\partial x} w_i \\ \frac{\partial N_i}{\partial z} v_i + \frac{\partial N_i}{\partial y} w_i \end{Bmatrix} = \sum_{i=1}^{4} B_i a_i^{(e)} = B a^{(e)} \tag{3.14}$$

in which B is the element strain matrix:

$$B = [B_1, B_2, B_3, B_4] \tag{3.15}$$

and B_i is

$$B_i = \frac{1}{6V^{(e)}} \begin{bmatrix} b_i & 0 & 0 \\ 0 & c_i & 0 \\ 0 & 0 & d_i \\ c_i & b_i & 0 \\ d_i & 0 & b_i \\ 0 & d_i & c_i \end{bmatrix} \tag{3.16}$$

Through Equation 3.16 it is possible to conclude that the strain matrix is constant.

3.2.2 Equilibrium equations

Considering the Equation 3.6, the PVW for a single element is [42]

$$\int\int\int_{V^{(e)}} \delta\varepsilon^T \sigma dV = \int\int\int_{V} \delta\mathbf{u}^T b dV + \int\int_{A} \delta\mathbf{u}^T t dA + [\delta a^{(e)}]^T q^{(e)} \tag{3.17}$$

in which $q^{(e)}$ is the vector of equilibrating nodal forces for the element acting on the virtual nodal displacements $\delta a^{(e)}$, with

$$\delta a^{(e)} = \begin{Bmatrix} \delta a_1^{(e)} \\ \delta a_2^{(e)} \\ \delta a_3^{(e)} \end{Bmatrix} \quad , \quad \delta a_i^{(e)} = \begin{Bmatrix} \delta u_i \\ \delta v_i \\ \delta w_i \end{Bmatrix} \quad , \quad \delta q^{(e)} = \begin{Bmatrix} \delta q_1^{(e)} \\ \delta q_2^{(e)} \\ \delta q_3^{(e)} \end{Bmatrix} \quad , \quad \delta q_i^{(e)} = \begin{Bmatrix} \delta F_{x_i} \\ \delta F_{y_i} \\ \delta F_{z_i} \end{Bmatrix} \tag{3.18}$$

The virtual displacements and the virtual strains are interpolated in terms of the virtual displacement through

$$\delta u = N \delta a \quad , \quad \delta\varepsilon = B \delta a \tag{3.19}$$

Substituting the equations 3.19 into 3.17, gives after rearranging the equation [42]

$$\int\int\int_{V^{(e)}} B^T \sigma dV - \int\int\int_{V^{(e)}} N^T b dV - \int\int\int_{A^{(e)}} N^T t dA = q^{(e)} \tag{3.20}$$

Introducing the equation 3.3, it is obtained the equilibrium equation for the element in the standard matrix form [42]

$$\begin{aligned} &\left(\int\int\int_{V^{(e)}} B^T D B dV\right) a^{(e)} - \int\int\int_{V^{(e)}} B^T D\varepsilon^0 dV + \int\int\int_{V^{(e)}} B^T \sigma^0 dV - \\ &- \int\int\int_{V^{(e)}} N^T b dV - \int\int\int_{A^{(e)}} N^T t dA = q^{(e)} \end{aligned} \tag{3.21}$$

or just

$$K^{(e)} a^{(e)} - f^{(e)} = q^{(e)} \tag{3.22}$$

where K is the stiffness matrix and $f^{(e)}$ is the equivalent nodal force vector for the element, with contributions from body forces, surface tractions, initial strains and initial stresses.

By assembling the contributions of $K^{(e)}$ and $f^{(e)}$ for each element, it is possible to obtain the global system of equations $Ka = f$.

Chapter 4

INEGI's Benthic Lander

INEGI's benthic lander, represented in Figure 4.1, was projected to act as a tripod, so it could adjust to the irregularities of the ocean floor. The design of the lander was developed in order to reduce the projected area, and thus, the drag during the deployment. Another priority taken into account was its modularity in order to simplify the replacement of both broken and specialized parts [43].

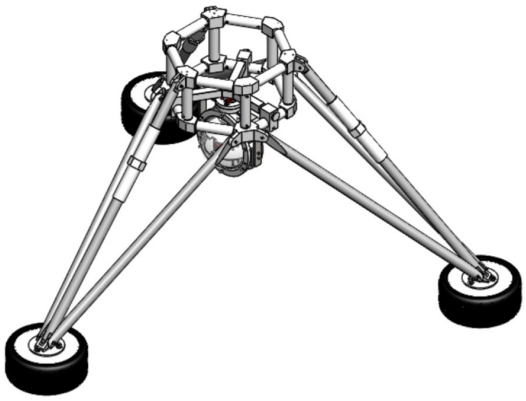

Figure 4.1: Model of INEGI's lander [43].

4.1 Lander description

The lander is essentially composed of five parts:

- The cage made of POM, which is the main structure of the lander;
- A glass sphere coupled to a structure made of POM where data collecting equipment is kept;
- The rods produced in POM;
- The feet made of POM;

- The ballast weights that consist of three pieces of concrete enclosed in a tire casing.

Each part, except for the ballast weights, is represented in Figures 4.2 to 4.5.

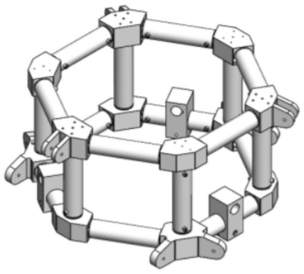

Figure 4.2: Lander's hexagonal cage [43].

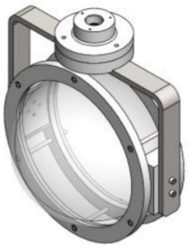

Figure 4.3: Lander's Sphere [43].

Figure 4.4: Lander's rods [43].

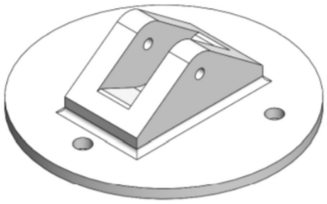

Figure 4.5: Lander's feet [43].

For the AMALIA project, the lander is expected to go as deep as 200 m. However, the material used allows it to reach 4000 m deep, only requiring to adjust the glass sphere and the ballast weights, so that the lander can be used in other activities [36].

Currently, the ballast weights are fixed to the feet of the lander through screws. So, until now, there were only deployments made in order to test the lander in the ocean. Both the deployment and recovery needed human labor. Currently, it is being developed a project with the aim to change the release method into an acoustic command or a timer, to avoid the requirement of human labor.

The lander was made using ERTACETAL C, commercial name of polyoxymeth-179 ylene (POM). This material was chosen mainly because of its low density and satisfactory mechanical properties [36], as described in section 2.7.

The lander is equipped with a spectral camera, a micro PC that controls the camera and is used to storage the data, a light source and integrated time switches to turn the equipment on and off during the trial. Due to the lack of space in the sphere, the batteries were packed in a watertight enclosure and kept alongside the structure [36], as can be seen in Figure 4.6.

In order to expand the horizons of the uses of the lander, it is crucial to develop a propulsion system module, so the lander can move underwater. This will allow to cover a greater area in a single deployment.

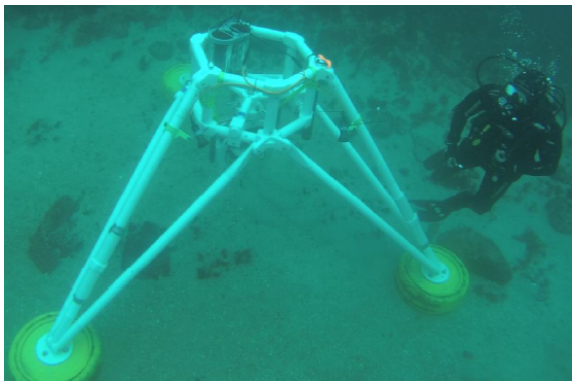

Figure 4.6: AMALIA lander in a sea trial [36].

Regarding mobility, the main concerns for the requirements of a mission are:

- Maximum depth of 200 m;
- Maximum velocity of 1 m/s;
- Total time of mission of approximately 30 days;
- The lander must be able to move in both vertical and horizontal directions.

For the design of the propulsion system, the maximum depth established was 200 m and not 4000 m as the rest of the lander. This is due to the fact that at that depth, the lander is withstanding very high loads and so, the lander as is now, would not be capable of withstanding loads caused by a propulsion system. Thus, it is considered to work at the required depth of 200 m and afterwards, future iterations can focus on adapting the system for greater depths.

4.2 Relevant information and calculations

In this section is presented relevant data to the project, regarding the weight of the structure - Table 4.1 -, the properties considered for the ocean - Table 4.2 - and calculations for the development of the project - Equations 4.1 to 4.3.

Table 4.1: Amalia's lander components' mass [43].

Part	Mass (kg)
Sphere	55,00
Cage	49,00
Rods (with feet)	31,00
Auxiliary equipment	70,00
Ballast weights	$3 \times 118,20$
Other equipment	6,40
Total	566,00

Table 4.2: Data about the lander and the environment in which it will operate [43].

Data	
Mass (m)	566,00 kg
Fluid density (ρ_f)	1025,00 kg/m^2
Lander volume (V_l)	0,30 m^3
g	9,81 m/s^2

By Newton's second law, it is possible to calculate the real weight (R) of the vehicle:

$$R = m \times a = 566,00 \times 9,81 = 5550,20N \tag{4.1}$$

By Archimede's principle is possible to calculate the buoyancy (B):

$$B = \rho_f \times g \times V_l = 1025,00 \times 9,81 \times 0,30 = 3015,30\text{N} \tag{4.2}$$

And the wet weight (W_w):

$$W_w = R - B = 5550,20 - 3015,30 = 2534,90\text{N} \tag{4.3}$$

In Figure 4.7 it is possible to see the dimensions and different options of use of the lander.

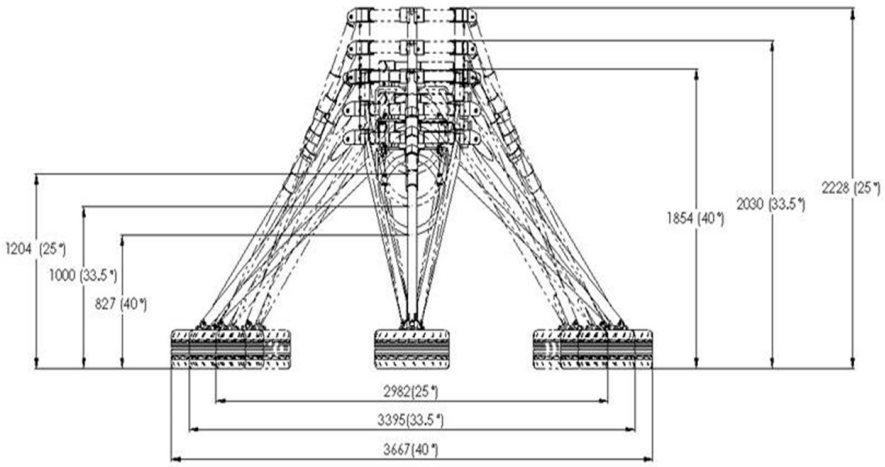

Figure 4.7: Amalia's dimensions in different set-ups [43].

Chapter 5

Mobility in underwater vehicles

Underwater vehicles' movement can be simplified and decomposed into a 2-dimensions movement. This way, the movement can be split into two different components, one vertical and another horizontal. To achieve movement in each of these ways, different systems can be used. For vertical movement can be used Variable Buoyancy Systems (VBS) . The vehicles can vary their buoyancy and adjust it to the desired depth, getting neutral buoyancy and therefore it is not necessary to constantly have the system working during the mission. For the horizontal movement are used propulsion systems that make the vehicle circulate, once it gets neutrally buoyant. Both are explained in the next sections and are also given examples of different systems.

5.1 Variable buoyancy systems

Accordingly to the Archimede's Principle, an upward force called buoyancy acts in a body emerged in a fluid, due to the hydrostatic pressure and is equal and opposite to the weight of the fluid displaced [44]. This can be expressed through the equation

$$B = \rho \times g \times V_d \tag{5.1}$$

in which B, ρ , g and V_d stand for buoyancy, fluid's density, gravitational acceleration and volume of fluid displaced.

In a body submersed in a fluid act two main forces in the vertical axis: weight and buoyancy. In this section are presented systems that allow to vary the intensity of these forces acting in an underwater vehicle and therefore change its vertical position.

5.1.1 Discharge variable buoyancy system

This system has been perfected through experience and is very effective at changing buoyancy in one-way. However, this method can only affect buoyancy in increments correspondent to the weight of the pieces that are dropped, and implies leaving material in the oceans and therefore

wasting these pieces and the money spent on them, while also contributing to marine pollution [45].

5.1.2 Flexible ballast tank system

Pneumatic solutions can also be used for VBS. In these cases, there are usually tanks with pressurized air that can be transferred to a flexible ballast tank, in order to increase its volume and thus its buoyancy. In order to decrease volume of the flexible tank, air can be threw out through valves [46].

This is a fairly simple solution, however, the variation of the buoyancy is limited to the volume of compressed air available.

5.1.3 Pumped water variable buoyancy system

This system, represented in Figure 5.1 is composed of a pressure tank and regulates the buoyancy of the vehicle by varying the volume of water inside of it and thus, adding or removing weight. In order to accomplish this, the system is also composed of a set of valves and a pump [45].

This system presents high freedom in what comes to design, so it can be engineered accordingly to the necessities of a vehicle. However, it is limited by the power available and the energy requirements increase with depth [45]. It is also limited to the volume of the tank: it cannot get lighter than when it is empty, nor heavier than when it is full.

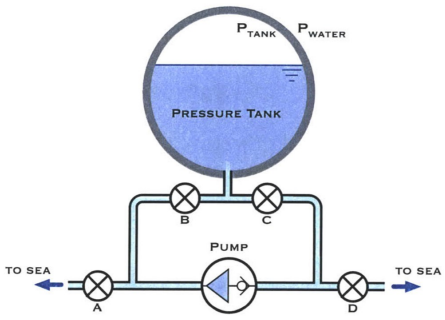

Figure 5.1: Scheme of a pumped water variable buoyancy system [45].

One-way tank flood VBS is similar to the pumped water VBS, the difference is that during the mission it can only be flooded, increasing the weight of the vehicle and decreasing the buoyancy. However, it can still be emptied after being recovered and reused in future dives [45].

5.1.4 Pumped oil variable buoyancy system

The pumped oil VBS is commonly used to achieve repeatable, two-way buoyancy changes.

This system, represented in Figure 5.2 a), relies on the change of buoyancy of the vehicle, by changing the volume of a compartment and therefore, the volume of water displaced. In order to achieve this, oil is pumped from inside a pressure housing to an external flexible bladder. Then, the buoyancy can be reduced by opening a valve and the oil is forced back to the reservoir [45].

This system is characterized by its reliability and because it can be repeated many times, being only limited by the power available. The use of oil instead of seawater, allows to reduce the risk of pump malfunctions. This system is usually chosen for vehicles that require long missions or small buoyancy changes. However, oil must be conserved in a pressure housing and there must be space for the bladder expansion. This may mean a system that is too large for smaller vehicles and thus, inappropriate to use in these cases. The rate of buoyancy change is dependent on pump speed and it must be taken into account that pump's power consumption increases with depth [45].

The piston-driven oil VBS, represented in Figure 5.2 b) is very similar to the pumped oil VBS. The difference is that instead of using a pump, it uses a piston. The piston is usually controlled with a motor and screw mechanism. These, however, must also be kept in a pressure housing. This may require a higher volume system, which can have a negative impact in the desired buoyancy of the vehicle. However, by using a piston, the risks associated with a pump, such as particles or gas bubbles, are minimized [45].

a) b)

Figure 5.2: Representation of: a) pumped oil VBS b) pumped oil piston VBS [45].

5.2 Thruster systems

The thruster system takes the energy from the power source and converts it into thrust for propelling the vehicle. It is composed of two parts: power transmission system and propulsor system [47]. In the next sections are explained some of these systems, as well as their advantages and disadvantages.

5.2.1 Power transmission system

The power transmission system can be either: direct mechanical drive with or without reduction gears, hydraulic pump and motor drive or electric drive [47].

Direct mechanical drive with reduction gears is an option mostly used in surface ships and submarines. These are used in order to adapt the high speed of a prime mover and the lower speed required for optimum efficiency of the propeller.

The use of reduction gears usually mean high noise levels and increased weight. Another concern regarding the use in submersible vehicles is the shaft seal, in what comes to maintenance

and reliability. The general use of this type of mechanical drive is due to the ability to transmit very high levels of power with acceptable efficiency.

The use of a mechanical drive without reduction gears is rarer, since the speed of the prime mover and of the propulsor must match. This does not seem to be a viable option for relatively small submersible vehicles [47].

Another option is the usage of an hydraulic pump and motor drive. This system requires a battery to power an electric motor that drives the pump. This, in turn transmits hydraulic pressure to an hydraulic motor, which is used to drive the propulsor shaft. As a result of the losses associated to the energy conversion and transmission, the system efficiency is highly affected. Thanks to this, hydraulic solutions are used for cases in which electric motors cannot provide sufficient thrust or when the vehicle needs an hydraulic system for other purposes, such as manipulators [47].

An hydraulic system requires the use of valves, compensators, among other equipment, contributing to the increase of the vehicle's weight. Besides, it presents the risk of leaking fluid harmful to the environment and ecosystems. However, an advantage of these systems is that it is only needed one prime mover.

All-electric propulsion systems with externally mounted electric propulsion motors are the most used for small submersible vehicles. This is due to their efficiency and the flexibility in arrangements provided by the use of electric systems. By using external mounted motors, there are no problems associated with sealing a rotating shaft penetrating the pressure hull of vehicles [47]. In opposition to the hydraulic systems, each electrical equipment needs a motor which can lead to a heavier system if several motors are required [11].

5.2.2 Propulsor system

The screw propeller is the most used system in ship propulsion. It is used in a variety of configurations and designs. Two of them are presented in this section.

The open propeller, represented in Figure 5.3, is the simplest design for a propeller. since it does not have any kind of shroud, it is more prone to damage and fouling, but also present simple production.

The shrouded propellers, represented in Figure 5.4, consist in a ring is placed around the propeller, concentric to it, which increases its efficiency. An advantage of this configuration is the possibility of achieving high thrust at low speed.

5.3 Electric thrusters in underwater vehicles

As stated previously, electric thrusters are the most used solution for underwater vehicles of small and medium sizes. In this section are presented some concerns that should be taken into account in what comes to the use of thrusters.

Electric thrusters provide more accuracy and a faster response. If it is not a problem that the vehicle has to move horizontally in order to move vertically the vehicle can also use a single

Figure 5.3: Open propeller [48].

Figure 5.4: Shrouded propeller [48].

thruster for both the horizontal and vertical movement with the use of diving planes or a robotic wrist [49]. However, some AUVs can have 3 thrusters units: for the main propulsion, for hovering and for auxiliary propulsion. The hovering unit is used in order to maintain the constant depth [47].

5.3.1 Arrangement and movement

The arrangement of the thrusters in a vehicle allows to achieve different types of movements. In this chapter are presented aspects that must be considered in the arrangment of thrusters on ROVs and are suggested and evaluated options for the lander of the project.

In underwater vehicles, the thrusters must be positioned so that the moment arm relatively to the center of mass allows a proper maneuverability. Furthermore, different kinds of movement can be achieved by varying thruster output and asymmetrical thrusting, thus the importance of the arrangement of the thrusters.

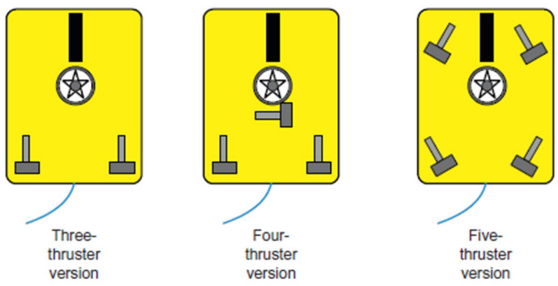

Figure 5.5: Main arrangements for thrusters in ROVs [11].

There are three main set-ups, which are represented in Figure 5.5:

- The three-thuster arrangement, which only allows the vehicle to fore, aft and yaw;
- The four thruster version, that also grants the possibility of lateral translation;
- The five-thruster configuration allows to thrust in any horizontal direction. With multiple vertical thrusters further allows for pitch and roll function through asymmetrical thrusting.

The placement of the thrusters with an angle relatively to the vehicle longitudinal axis, as represented in Figure 5.6 also impacts the movement of the vehicle, allowing it to have a better turning moment and still provides longitudinal stability [11].

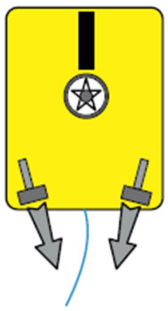

Figure 5.6: Thrusters aligned off the longitudinal axis [11].

Multiple horizontal thrusters operating along the same axis may cause an issue called torque steer. If the thrusters' propellers rotate in the same direction, then it is produced a counter-reaction to the turning moment, making the vehicle role. In order to avoid this and thus course deviations, underwater vehicles must have propellers that can operate in both directions. This situation is illustrated in Figure 5.7.

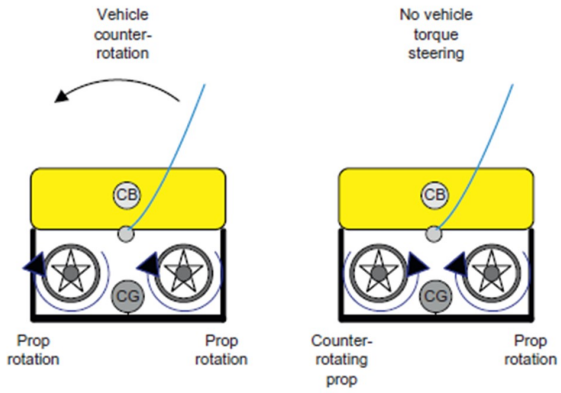

Figure 5.7: Torque steer and rotation of propellers [11].

The information presented is mainly regarding the concepts of thrusters and mobility applied to ROVs . It is therefore important to note the differences between them and the lander considered. An ROV has usually neutral buoyancy, while a lander has negative buoyancy while it is operating. The different kinds of operations present different requirements to the thrusters. While the ROVs circulate freely for long periods of time, in this project, the lander only needs to move from one place to another. Taking this into account, next are presented other options that can be more suitable for this project.

5.3.1.1 Tricopters and hexacopters

Underwater vehicles are similar to drones. After all, drones are vehicles that circulate freely in a fluid, being this fluid the only difference. Although it makes a considerable difference for a vehicle to circulate in air or water, the physical principals are the same, so the arrangement of the thrusters of underwater vehicles can be similar to those of drones. In this section are explained pros and cons of two types of drones: tricopters and hexacopters, that are useful to this project.

Tricopters present the advantage of being cheaper thanks to the reduced number of thrusters. However, there is no redundancy and if one of the motors, for some reason, stops working, the vehicle will likely crash. It also presents less stability than a drone with more thrusters. However, in the case of an underwater vehicle, that should not be a problem, since its positive buoyancy allows it to ascend to the ocean surface. If one thruster stops working during the movement of the lander, the impact caused when the lander reaches the seafloor may damage the structure. However, it should not be a difficult task to create a security feature in the control system of the lander that enables it to release the ballast weights when one of the thrusters stops working.

Hexacopters, contrarily to tricopters, present redundancy and in some cases, even losing two motors, the drone is capable of being controlled and not necessarily crashes. By having six motors, these do not need to be as powerful as in the tricopters. However, there are more arms and connections, so the system can get heavier.

SWITCHBLADE-ELITE is a tricopter, presented in figure 5.8, that is produced by Vision-Aerial and can be used for oil and gas inspection, precision agriculture, cinematography, among many other applications. This tricopter can withstand a maximum payload of 2,3 kg, can reach velocities of 100 km/h and resist winds up to 13,3 m/s [50].

Matrice 600 PRO, presented in Figure 5.9, is a modular hexacopter produced by DJI directed to professional aerial imaging. It can reach 65 km/h and resist to winds up to 8m/s. Although each motor can generate a thrust force of 5,1kg, it is advised for the drone to only support equipment up to 15,5 kg [51].

Figure 5.8: SWITCHBLADE-ELITE [50].

Figure 5.9: Matrice 600 PRO [51].

Chapter 6

Design

In this chapter, after an analysis of the case, the propulsion system is chosen and the design process is developed and explained.

6.1 Project requirements

Below, are listed the requirements taken into account in the development of the project. For each item, the first letter R or D stand respectively to required or desirable.

- R - The thrusters must be able to completely propel the vehicle, not depending on other features;
- R - Modular solution;
- D - Low projected area in the horizontal plane and in the plane perpendicular to the currents in order to achieve low drag in both directions.

6.2 Analysis of the case

Firstly, the possible paths of the lander when in motion between two positions were schematized, as can be seen in Figure 6.1.

It was then made an analysis of the forces and in Figures 6.2 and 6.3 are presented the forces acting on the lander during the movement and while static.

The forces W,B,C,T and BW represent respectively the forces associated to weight, buoyancy, current, thrust and ballast weights. Even though that at the projected operating depths the currents can be considered negligible, they are still represented in the diagrams.

6.2.1 Choice of the propulsion system

As explained in chapter 4 the lander uses ballast weights, but this only allows the lander to move vertically and with just two available positions: the ocean floor and the ocean surface. In order to allow the lander to chance its location, a propulsion system must be projected.

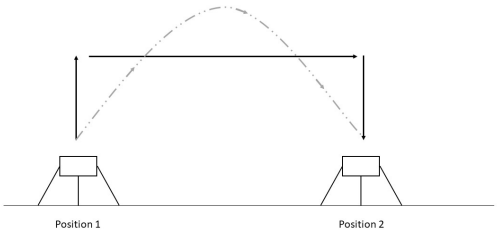

Figure 6.1: Possible paths of the lander between two positions.

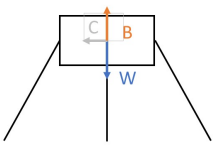

Figure 6.2: Free body diagram when the lander is static.

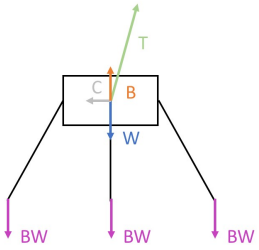

Figure 6.3: Free body diagram when lander is initiating motion.

With the information presented in the chapter 5, and because the lander does not have any hydraulic actuators, the use of hydraulic pump with motor drive is not considered suitable. This decision is taken mainly due to its low energy efficiency and the complexity of integrating an hydraulic system without affecting considerably the projected area of the lander and thus the drag. The pumped oil and piston-driven oil VBS also present this problem.

The one-way tank flood VBS presents the same disadvantage of only having two extreme positions, so it does not solve this adversity.

There are therefore three possibilities: either using a pumped water or a pneumatic VBS with at least two thrusters for horizontal movement, or use thrusters placed vertically and use the lander as an underwater drone, as explained in 5.3.1.1.

Due to the requirement that the thrusters must be able to propel the vehicle by themselves, not depending on other features, the only viable option is to only use electric thrusters.

If one of the solutions with a VBS and horizontal thrusters were to be chosen, these would have to be extremely powerful, in order to be able to thrust the lander vertically. As an alternative, there was also the possibility to use thrusters that could adjust their orientation. However, this would be too complex for a first approach of the propulsion system.

Between these possibilities, the choice made was to use thrusters and make the lander move as an underwater drone.

Even though keeping the ballast weights means an increase in the requirements of the thruster's power, they would just operate during the movement from one place to another. They do not need

to operate while the lander is in the ocean floor collecting data. Furthermore, the ballast weights are still needed so that the lander can descend freely to the ocean floor.

6.2.2 Choice of the arrangement

In order to reflect without much restrictions, there were firstly made sketches of the arrangement of the thrusters without taking into account the information presented. These options were then evaluated, considering the information. The main consideration in the development of these sketches, was to have in mind the symmetry of the lander. The results are presented in Figure 6.4.

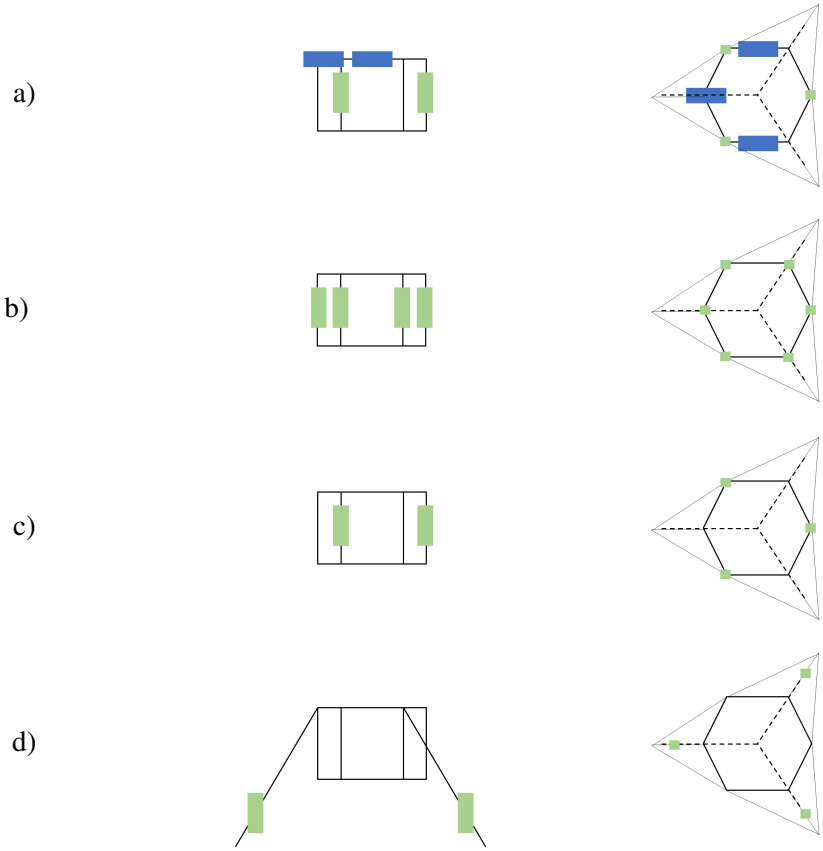

Figure 6.4: Front and top views respectively of four possibilities for thrusters' arrangement.

Through the elaboration of Table 6.1, an analysis was made based on four criteria: drag, reliability, spatial limitations and analysis security. These were given an evaluation between 1 that meant "not satisfying at all" and 4 that meant "very satisfying".

The drag column evaluates the impact on the drag of the vehicle. Option b) is in disadvantage, since there would have to be thrusters in the cage near the legs of the lander.

Reliability was rated in the eventuality of one of the thrusters failing, if the lander could still be recovered. Option b) is in advantage, since it has more thrusters. However, other options are not rated as a "1", since if a high coefficient of security is chosen, it can still be possible to recover the lander, even if the ballast weights needed to be released.

Spatial limitations evaluations regard the mounting of the thrusters in the lander. The horizontal thrusters for option a) would affect the space currently used for batteries, thus the evaluation made. Solutions b) and d) propose mountings in zones highly restricted by the set up of the legs.

For the analysis security, the margin of the loads considered was evaluated. Therefore, options that cause critical situations are valued. This way, even if adjustments are made in the future, the project developed can still be used. Since solution b) has six distributed thrusters, the effect would not be as critical as solutions c) and d), because the loads generated by each thruster would be inferior. However, solution a) presents three more thrusters in different zones of the lander, besides the vertical thrusters that option c) also considers, which could lead to a more critical scenario.

Another important factor is that option d) is the one that presents the highest distance between the center of mass and the thrusters, but that can be overcome in the other options, taking this into account during the design process.

Cost was not a factor taken into account, since it would be difficult to compare options which required less but powerful thrusters with others that suggested more and less powerful thrusters.

Table 6.1: Evaluation of the possibilities proposed.

Option	Drag	Reliability	Spatial limitations	Analysis security	Average
a	4	2	2	4	3
b	2	4	1	2	2,25
c	4	2	4	3	3,25
d	3	2	1	3	2,25

This evaluation allows to objectively choose option c), since it is the one that presents the highest average.

6.3 Thrusters' selection

For the thrusters' selection, it was considered the worst case scenario in which the lander would be stuck in mud or other sediments in the ground. For security, it was stipulated that the lander should be able to thrust two times its wet weight (571 kg) or its real weight (566 kg), whichever was the greatest. So, there is the requirement for the thrusters to generate at least 571 kg.

Furthermore, it is important to take into consideration the weight and the volume of the set of thrusters, since these will affect the buoyancy and the weight of the vehicle. Because of this, it might be useful to adjust the weight of the ballast weights or even increase the buoyancy of the lander. This is further discussed and evaluated in section 6.6.

Concerning the described factors and after contacting companies that commercialise thrusters, the Table 6.2 was made in order to compare the thrusters models found. However, there was no response from most of them regarding the price. In this table are also presented the weight required to the new ballast weights. Since the thrusters meant a heavier lander, then, it is not necessary to have ballast weights as heavy as projected before.

The first sketches and models for the connection were made taking into consideration the Technadyne 8020. The company was chosen because it was the only one that presented sufficient information to continue developing the project. Among its models, the 8020 was the one that presented the lowest energy consumption, but still ensured the thrust requirement presented before.

However, the price of the set is extremely high, so that is not a viable option financially speaking. Nonetheless, the focus of the dissertation is to design a propulsion system for the lander. So, this will be the considered thruster in the development. This issue will also be taken into account in the design, so that the solution can be easily adapted to others models.

Table 6.2: Thrusters' data [52, 53, 54, 55]

Brand	Model	Depth rating(m)	Thrust force(kgf)	Power (kw)	Voltage (V)	Mass/thruster (kg)	Number of thrusters	Total thrust(kgf)	N (Total thrust/ /total dry weight)	Thruster's mass (k)	New ballast weights (kg)	Unit price($)	Total price($)
Tecnadyne	8020	750	226	12,5	150-330	26,3	3	678	1,196611366	78,9	275,7	23000	69000
	8020	750	226	12,5	150-330	26,3	6	1356	2,393222732	157,8	196,8	23000	138000
	8040	750	167	12,1	150-330	23,5	6	1002	1,768443346	141	213,6	23700	142200
	8050	750	182	8,7	150-330	47,6	6	1092	1,927285563	285,6	69	34500	207000
Copenhagen subsea	VXL	3000	244	32	24-800	17,8	3	732	1,291916696	53,4	301,2	No data	No data
	VL	3000	125	17,8	24-800	11,4	6	750	1,323685139	68,4	286,2	No data	No data
Lian innovation	240T 400-080	500	265	11	No data	16,8	3	795	1,403106248	50,4	304,2	No data	No data
	240TH 500-080	500	214	8,5	No data	16,8	3	642	1,133074479	50,4	304,2	No data	No data
	180CH-300-080	500	407	30	No data	No data	3	1221	2,154959407	No data	No data	No data	No data
	180ES-298-078	500	132	9,5	No data	No data	6	792	1,397811507	No data	No data	No data	No data
Integrated Thruster	300mm	11000	255	19	150	25	3	764,5259939	1,349322262	75	279,6	No data	No data

6.4 Thrusters' connection to the lander

The connection between the lander and the thrusters was designed in order to be as universal as possible. This way, even if later another thruster is chosen, the connection can still be used.

The most common design feature of thrusters is the cylindrical shape, so this was taken into consideration in the first steps of the development of the design of the connection.

In a document provided by the company, various options to mount the thrusters are proposed. Among them, the two solutions presented in Figure 6.5 are the most simple and adequate to the lander. Besides, none of them require a special order and therefore, no additional cost.

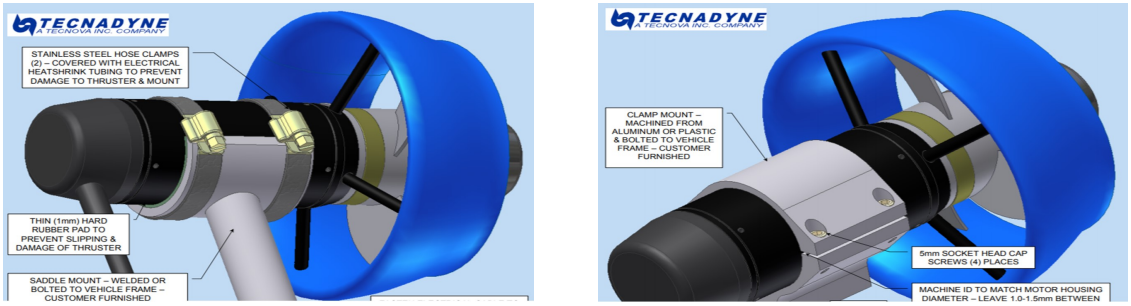

a) b)

Figure 6.5: Mountings proposed in the guide with a) stainless steel hose clamps b) clamp mount [48].

However, the solution presented in Figure 6.5 a) does not suit the project, since the lander is for use in salt water and the clamps are easily corroded.

The initial approaches were then made with basis on Figure 6.5 b).

6.4.1 Loads

At this point, it was considered that there was only a vertical force generated by the thrusters.

For security, instead of using the initial thrust force considered, it was used the maximum thrust force that could be generated by one single thruster. It was also considered a security factor of 2, so that, even if one of the thrusters stops working and the lander gets stuck in mud, it is possible for the lander to take off the ocean floor. By detaching the ballast weights, it would then be possible for the lander to get to the ocean surface, thanks to its positive buoyancy, not depending on the three thrusters.

After these considerations, the loads considered were

$$T_z = 226 \times 2 = 452\text{kgf} = 4434\text{N}$$

At first sight, this value may seem excessively conservative, taking in account the real project loads. However, losing the equipment is not an option and thus, the project must be done so that it supports the most extreme situations imaginable.

6.4.2 Initial proposals for the design

After an analysis of the loads that would be generated by the thruster and actuate on the connection, some sketches were made in an initial approach, as can be seen in Figure 6.6.

In figure a) is represented the top view of the lander. The solution does not seem viable, once the thrusters are limited by the internal space of the cage of the lander. Furthermore, they are too close to the center of gravity, which would negatively affect the mobility of the lander.

Figure b) represents a viable but too simple solution, not providing much rigidity along the vertical axis. Figure c) presents an improvement, since it provides more rigidity to the connection.

Solution illustrated in image d) appears to represent the best solution rigidity wise. However, it also presents a higher difficulty of assembly. It can also affect the set ups of the legs of the lander, since three vertical tubes of the cage are needed for the assembly. Thus, it can ultimately affect the functions of the lander.

Taken these considerations into account, it was chosen to develop a solution based in figure c).

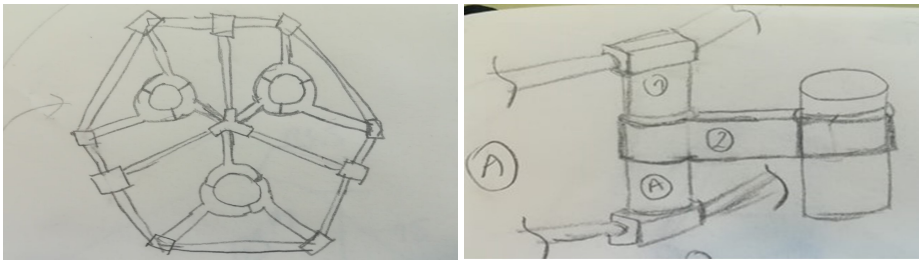

a) b)

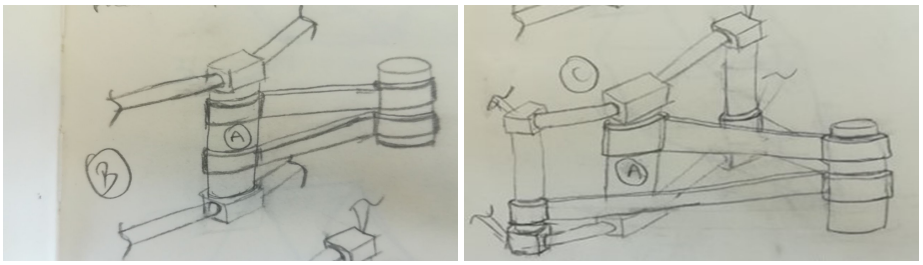

c) d)

Figure 6.6: First sketches of the mounting.

The design was developed and modeled in SolidWorks software and is represented in Figure 6.7.

6.4.3 Design development

After the initial simulations, many iterations were made, with the goal of reducing the mass and having in mind the intention to produce the item through machining.

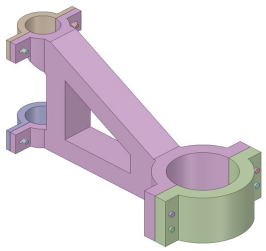

Figure 6.7: First model.

Thicknesses were reduced and one of the pieces was replaced with four others, making them easier to produce by machining. To join some of these pieces, it was suggested to use stainless steel bolts.

In the next iteration, the clamps were reduced, in order to not overcome the hexagon's contour. Other dimensions were adjusted so that the connection better fitted the lander. In order to support one of the superior clamps, some changes were made.

In the last iteration, some changes were done in the clamps, in order to prevent the system to rotate around the tube of the lander.

At last, the design was adapted to the diameter of the holes required for the screws calculated in the next section 6.5.

The evolution of the model, as well as final individual models of each designed piece are presented in Figures 6.8 to 6.13. It should be noted that the exterior clamps of the lander are similar, but slightly different from each other. This is due to the different geometry of the hexagons of the cage, with which each of one contacts.

Regarding the production of the pieces, all of them are easily obtained by machining. In order to avoid wasting material and thus costs, the material cut out of the interior of the main piece, represented in Figure 6.11, could be used to produce other pieces, such as the interior clamps of the lander, represented in Figure 6.9.

The final dimensions of each piece are presented in the drawings in Appendix B.

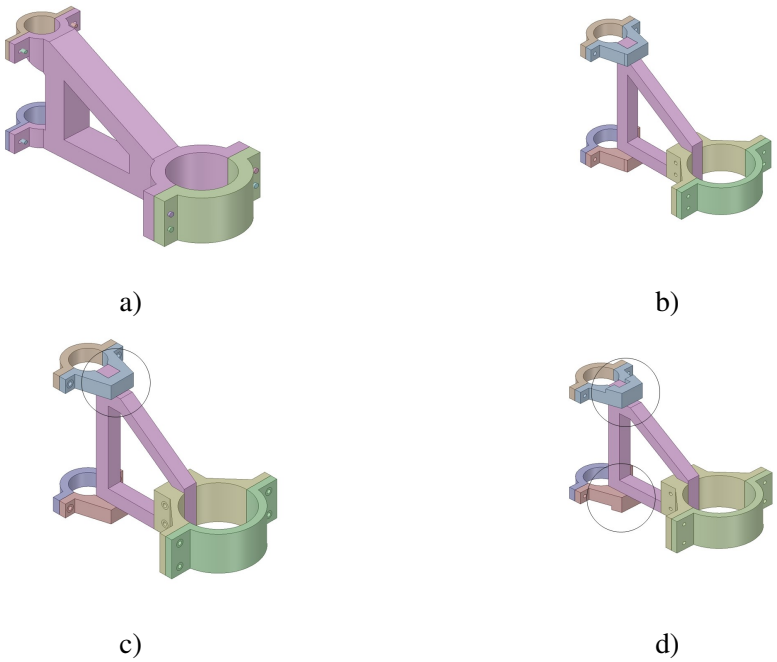

a) b)

c) d)

Figure 6.8: Evolution of the design of the mounting with highlights of the changes.

6.5 Dimensioning of the screws and washers

The calculations regarding the dimensioning of the screws were made recurring to the software PTC Mathcad Prime 6.0. Therefore, the calculations and considerations made can be consulted in Appendix A [56, 57].

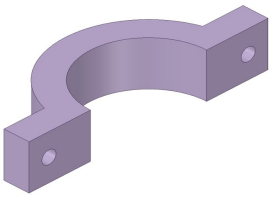

Figure 6.9: Interior clamp of the lander.

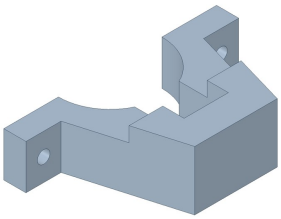

Figure 6.10: Exterior clamp of the lander.

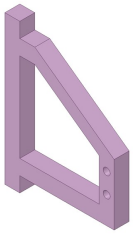

Figure 6.11: Main piece.

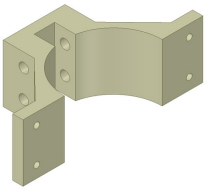

Figure 6.12: Interior clamp of the thruster.

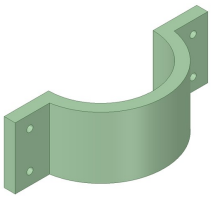

Figure 6.13: Exterior clamp of the thruster.

6.6 Buoyancy verification

As explained before, after choosing the thrusters and having an idea of how the connection will be made, there must be calculated if the vehicle still has positive buoyancy and will rise to the surface once the ballast weights are detached.

The weight and volume of the added items are presented in Table 6.3.

Table 6.3: Weight and volume data of added items.

	Weight (kg)	Volume (dm^3)
Thrusters	26,70	38,47
Connection pieces	0,95	0,67
Set (sum)	27,65	39,14
Total (3 sets)	82,95	117,43

As presented in section 4, the initial weight of the lander without the ballast weights is 205kg and the volume is 0,3 m^3.

Table 6.4: Weight and volume data of added items.

	Weight (kg)	Volume (dm^3)
Initial lander	205,00	300,00
Added items	82,95	117,43
Total	287,95	447,43

The initial and final weight forces W_i and W_f and the buoyancy B_i and B_f can be calculated through

$$W_i = m_i \times g = 205,00 \times 9,81 = 2011,05N$$
$$B_i = \rho \times g \times V_i = 1025,00 \times 9,81 \times 0,30 = 3013,50N$$
$$W_f = m_f \times g = 287,95 \times 9,81 = 2820,38N$$
$$B_f = \rho \times g \times V_f = 1025,00 \times 9,81 \times 0,45 = 4524,86N$$

And the buoyancy/weight proportions are:

$$\frac{B_i}{W_i} = \frac{3013,50}{2011,05} = 1,50$$
$$\frac{B_f}{W_f} = \frac{4524,86}{2820,38} = 1,60$$

By the increase in difference and proportion between buoyancy and weight, it is possible to conclude that the solution proposed does not affect negatively the buoyancy of the vehicle.

Chapter 7

Finite Element Analysis

7.1 Structural analysis

In this chapter are presented all the considerations taken in the model developed, as well as the results and their analysis.

For the structural analysis of the project was used the Ansys® Academic Research Mechanical, Release 20.2 license provided by FEUP.

7.1.1 Simplifications

The design of the CAD model of the lander was simplified in order to reduce the computational time. Chanfers were removed and the contacts between each piece were simplified. An example can be seen in Figure 7.1. This allowed to eliminate many small faces and edges regarding the connection of the tubes and hexagons, facilitating the generation of mesh and decreasing the solution time. These are acceptable modifications that do not present a significant change in an initial analysis of the results.

It was only considered one third of the lander due to its symmetry and the symmetry of the solution proposed, as can be seen in Figure 7.2, and the boundary conditions of this simplification were taken into account.

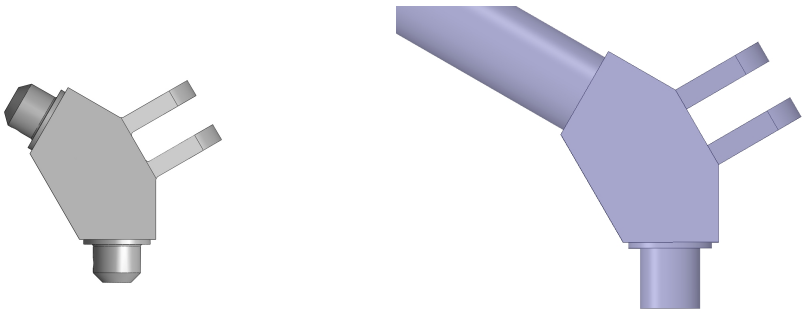

Figure 7.1: Comparison: before and after simplifications in a piece.

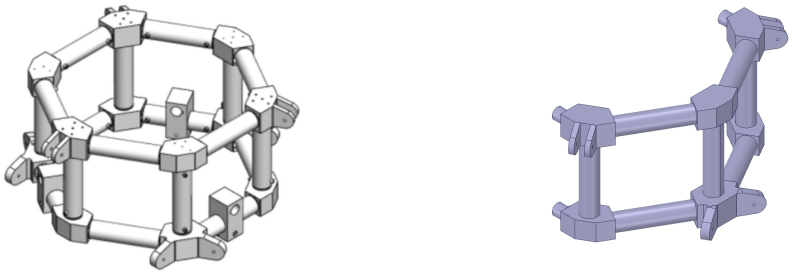

Figure 7.2: Structure of the cage and the part of it considered for the analysis.

7.1.2 Material

As stated in section 2.7, the material chosen for the project is POM. The material has been studied by INEGI, namely after long periods underwater. As expected, the properties of the material degraded. These can be consulted in Table 7.1.

Table 7.1: Properties considered for POM.

Property	Density (kg/m^3)	ν	E (MPa)	Bulk Modulus (MPa)	Shear Modulus (MPa)
POM	1410,00	0,38	3010	4180,60	1090,60

7.1.3 Mesh

The mesh of the model is composed of 254549 nodes and 71401 elements. In the generation of the mesh, it was given preference to hexa elements, thanks to the more simple approach to refine the mesh, as well as due to limitations of the license of the software used. The element order was set to linear. The mesh presented an average value of skewness of 0,49 and an aspect ratio average of 4,25.

7.1.4 Loads

Another analysis of the loads generated by the thruster was made. Firstly, it was generated a mass that represents the thruster's mass. Regarding the loads generated by the thruster, for security, it was considered that during its operation, there was the possibility for the thruster to rotate 5º and thus produce a force in the horizontal direction.

The components of the thrust force T are, accordingly to the referential used in Figure 7.3, therefore:

$$T_z = 452 \times sin(5^o) = 39,39\text{kgf} = 386,5\text{N}$$
$$T_y = 452 \times cos(5^o) = 450,28\text{kgf} = 4417,3\text{N}$$

The described loads act on the faces that contact with the thruster, highlited in red in Figure 7.3.

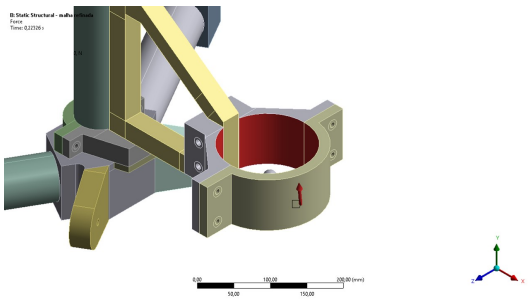

Figure 7.3: Faces in which the loads of the thruster act.

It was also necessary to take into account the hydrostatic pressure acting on the equipment. As the lander is projected to go as deep as 200 m, this was the depth considered.

Since the lander will circulate underwater, above the ocean floor, the ballast weights will cause a force in the ears of the hexagons of the cage. It is then needed to consider a remote force, that acts on the faces of the connection between the lander cage and its legs, pictured in Figure 7.4. For this force the weight considered was the value previously calculated in Table 6.2 for the first row, that corresponds to the thrusters' choice, and is therefore $275,70/3 = 91,90$kg.

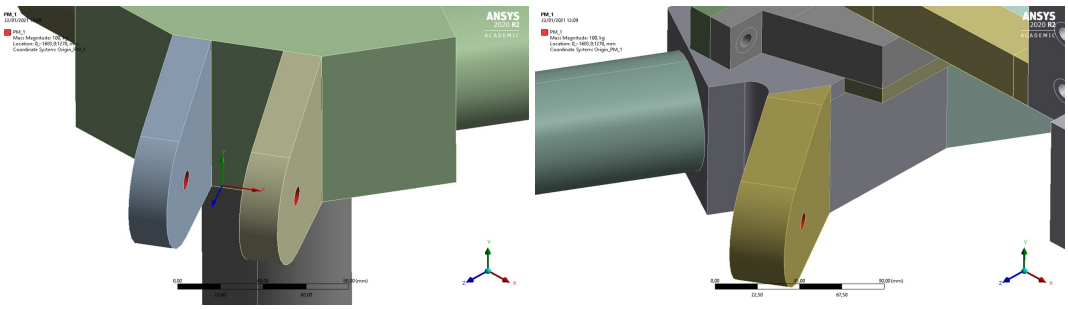

Figure 7.4: Faces where the force of the ballast weights acts.

7.1.5 Considerations in the analysis

The bolts were modeled as a circular beam with a diameter equal to the diameter of the hole. However, the M14 bolts were modeled with a mesh, since it was not possible to generate a beam, in which both ends were attached to the same body, as is the case. All of them were set to be stainless steel bolts.

In the connections between the third of the cage of the lander under analysis and the rest of it, it was considered to be fixed supports. This, however, leads to a problem: the deformation results cannot be analysed, because the results will not correspond to the real case. In reality, the lander will move and therefore, the deformation caused by these fixed supports will not happen, because they will not be fixed.

7.2 Results

In this section the results of the simulations made are presented, regarding the considerations presented, in the structure and in the pieces that presented more critical results, as can be seen in Figures 7.5 to 7.10 and Table 7.2.

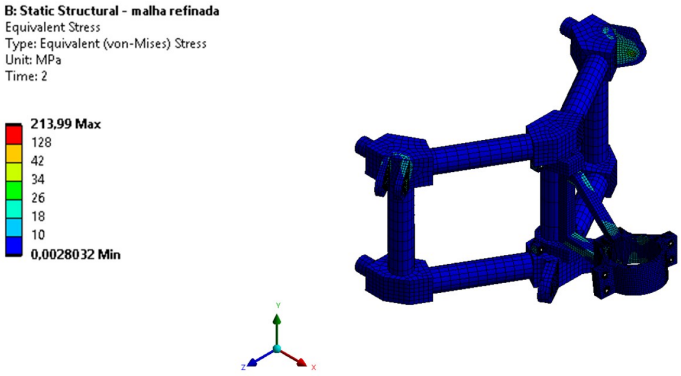

Figure 7.5: Result of the structure.

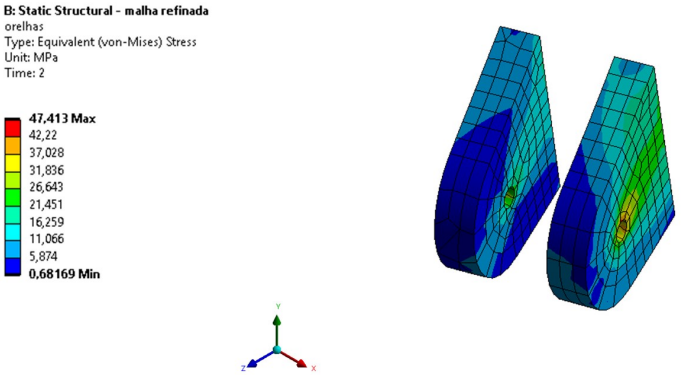

Figure 7.6: Result of the ear.

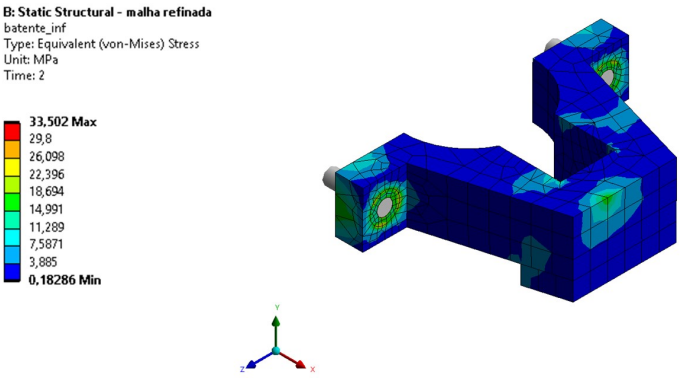

Figure 7.7: Result of the exterior clamp of the lander.

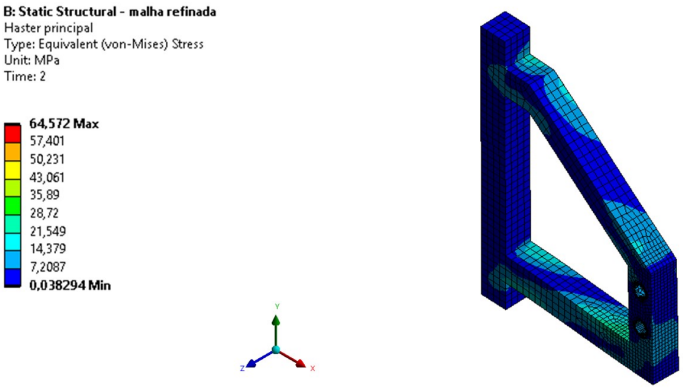

Figure 7.8: Result of the main piece.

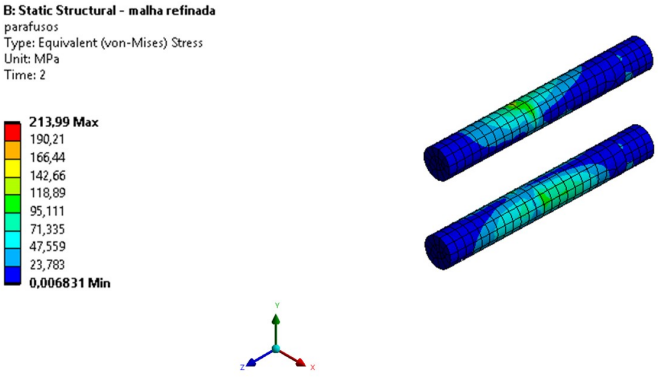

Figure 7.9: Result of the bolts.

.

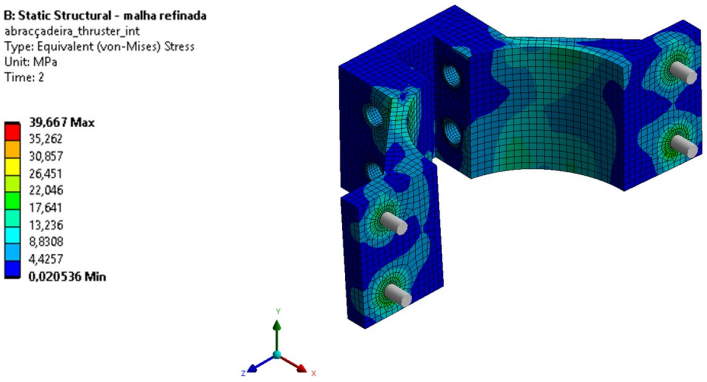

Figure 7.10: Result of the interior clamp for the thruster.

Table 7.2: Summary of the results

Piece	Maximum stress (MPa)
General	213,99
Ear of hexagon	47,41
Main piece	64,57
Bolts	213,99
Thruster's clamp	39,67

7.3 Analysis of the results

Before analysing the results, it is important to recall the values considered for the maximum values accepted in the project for POM, that take into account a security factor of approximately 1,43.

$$\sigma_{max_c} = 0,7 \times \sigma_c = 0,7 \times 72 = 50,40\text{MPa}$$
$$\sigma_{max_y} = 0,7 \times \sigma_y = 0,7 \times 66 = 46,20\text{MPa}$$

As can be seen in Table 7.2, the individual pieces presented, reach values of stress very close to the limits regarded as acceptable in the project.

Taking in account the limitations regarding the generation of mesh of the version of Ansys software used, the sub modeling method was used. This allowed to further evaluate the pieces that presented concerning values. For reference, the zones that were studied in depth, besides the ears, are represented in Figure 7.11.

7.4 Sub modeling

Sub modeling is a finite element modeling technique based in Saint Venant's principle: "altering a pressure distribution without affecting the resultant force results in a new stress field which is only significantly different in the neighbourhood of the changes" [58].

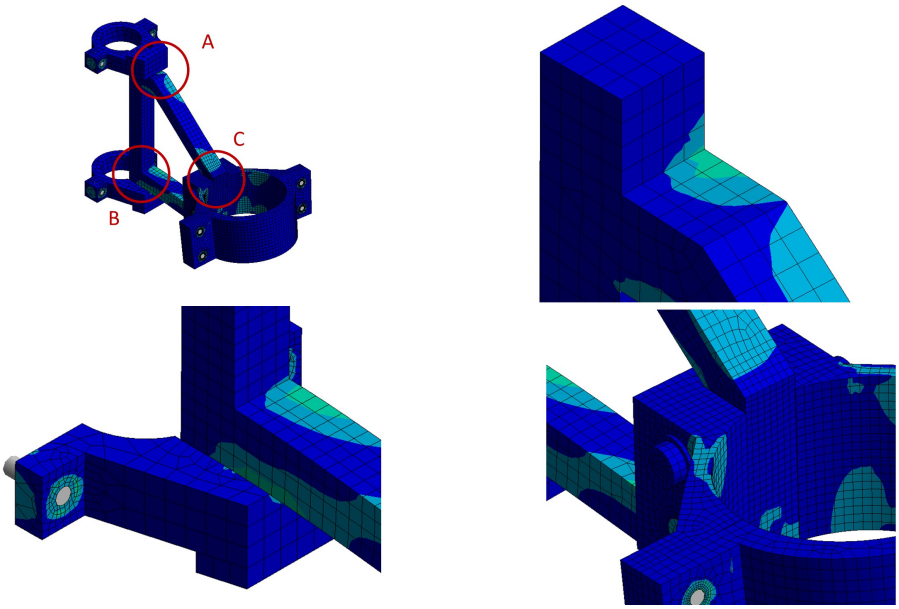

Figure 7.11: Identification of the zones analysed through submodeling.

This method consists on analysing a smaller part of the general model. By cutting it and focusing in a specific part of the finite element model, this method allows to deepen their analysis. The boundary conditions related to the cut of the model are transferred to the smaller model and the mesh is refined.

In Figures 7.12 to 7.15 are presented the sub models of the critical pieces. The increase of the maximum stress is explained by the Saint-Venant's principle: the consideration of the equivalent force in a new more refined mesh affects the behaviour, but only in the areas close to the cut and consequently, where the equivalent loads are applied. So, labels were put in the sub models, with the highest value of stress. These are the values relevant to considerate in the analysis, and not the highest presented in the scale.

Analysing the Table 7.3 that aggregates the results of the sub models, it is possible to conclude that the critical pieces of the structure are the ear, the main piece and the interior clamp of the thruster. In order to overcome the high stresses in the ear, it may be useful to study an increase of their thickness. It could also be considered a decrease in the ballast weights and consequently, the load acting on them. In the main piece and in the interior clamp of the thruster, the stresses generated are undoubtedly high and might present a problem in the project. However, for simplicity, the model presents sharp edges that should not correspond to the real production of the pieces. The production must take into account these edges and round them, allowing to avoid high tensions. So, a model closer to this must be developed in order to evaluate if the high tensions remain present.

Most critical areas evaluated are due to the reduced rigidity of the mounting along the Z axis. Therefore, other designs such as the d) sketch presented in Figure 6.6, should be explored and would definitely help to decrease the stress in the areas considered.

Table 7.3: Results of the submodels' analysis.

Piece/Zone	Maximum stress (MPa)	Number of nodes	Number of elements	Skewness average	Aspect ratio average
Ear of hexagon	83,06	101228	28959	0,38	3,34
Zone A	73,09	197046	50036	0,24	2,18
Zone B1	35,53	183116	47897	0,29	2,35
Zone B2	46,65	183116	47897	0,29	2,35
Zone B3	33,28	183116	47897	0,29	2,35
Zone C1	48,25	167897	43048	0,36	3,37
Zone C2	52,21	167897	43048	0,36	3,37
Zone C3	41,27	123398	34489	0,36	2,86

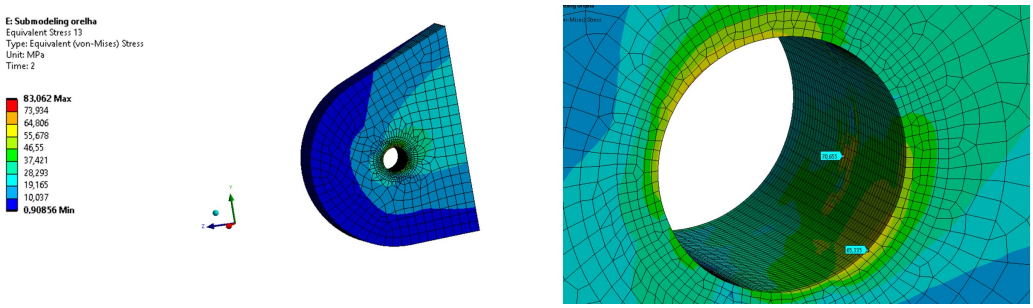

Figure 7.12: Results of the submodeling of the ear and close up of the critical area.

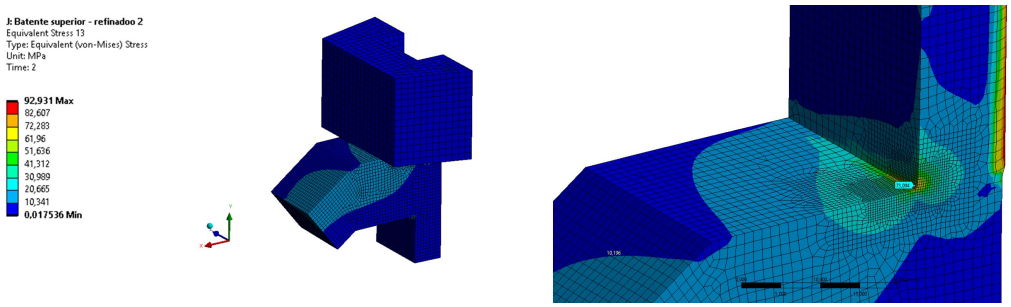

Figure 7.13: Results of the submodeling zone A.

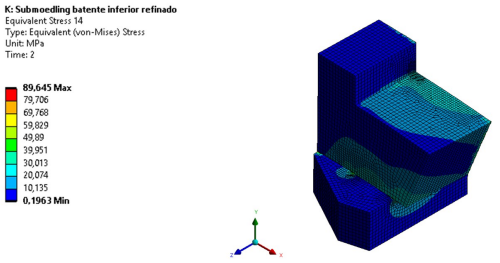

a) Zone B

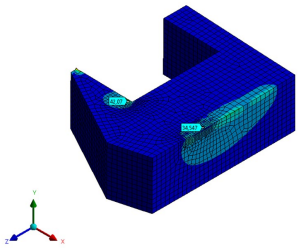

b) Zone B1

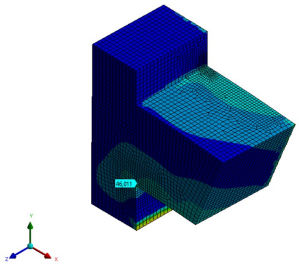

c) Zone B2

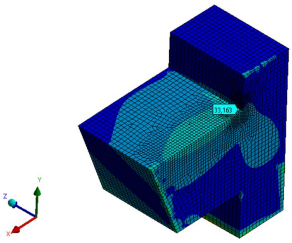

d) Zone B3

Figure 7.14: Results of the submodeling of zone B.

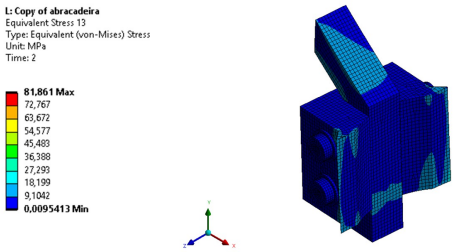

a) Zone C

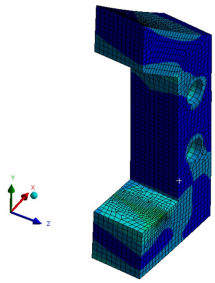

b) Zone C1

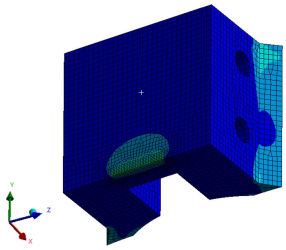

c) Zone C2

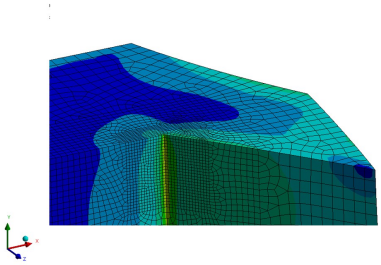

d) Zone C3

Figure 7.15: Results of the submodeling of zone C.

7.5 Modal analysis

A modal analysis is a requirement when projecting a structure. It is vital, in order to determine the vibration characteristics of the structure, namely the natural frequencies and mode shapes. Natural frequencies are the frequencies that the structure vibrates after it is disturbed, while mode shapes are the patterns of deformation of the structure at certain natural frequencies. It is undesired that the structure vibrates at these frequencies, once it provokes unwanted noise and mechanical stress and strain which leads to premature fatigue failure [59].

Starting with the basic equation of motion:

$$[M]\{\ddot{u}\} + [C]\{\dot{u}\} + [K]\{u\} = \{f(t)\} \tag{7.1}$$

where:

- $[M], [C]$ and $[K]$ represent respectively the mass, damping and rigidity matrices
- $\{\ddot{u}\}, \{\dot{u}\}$ and $\{u\}$ represent acceleration, velocity and displacement vectors
- $\{f(t)\}$ represent a load.

As both mode shapes and natural frequencies are a structure's properties and independent of loads, $\{f(t)\}$ can be assumed to be 0.

Considering an undamped system, is obtained:

$$[M]\{\ddot{u}\} + [K]\{u\} = \{0\} \tag{7.2}$$

Treating this as a frequency domain problem, and so assuming harmonic motion for every point of the structure:

$$\{u\} = \{\phi\}_i sen(\omega_i t + \theta_i) \tag{7.3}$$
$$\{\ddot{u}\} = -\omega_i^2 \{\phi\}_i sen(\omega_i t + \theta_i) \tag{7.4}$$

where ϕ, ω, t and θ represent respectively the amplitude, angular frequency, time and phase angle.

Substituting 7.3 and 7.4 in 7.2, it is obtained:

$$\{\phi\}([K] - \omega_i^2[M]) = \{0\} \tag{7.5}$$

which can be solved through

$$det([K] - \omega_i^2[M]) = \{0\} \tag{7.6}$$

which allows to obtain the angular frequency ω_i, that can be converted to Hertz through

$$f_i = \frac{\omega_i}{2\pi} \tag{7.7}$$

Once the angular frequency ω_i is known, it is possible to obtain $\{\phi\}_i$ that is the mode shape corresponding to the angular frequency.

A modal analysis was made for the whole structure of the cage and the mountings of the thrusters. The fixed supports were set in the connection between the cage and the legs of the lander. In Table 7.4 are presented the natural frequencies obtained.

The thrusters considered in this project can function up to 1500 RPM, which corresponds to 20 Hz. As the structure is projected to operate underwater, the natural frequencies are expected to be slightly lower [60]. However, they should not get as low as the frequencies of the thrusters and thus their use should not be a problem for the structure.

The mode shapes are presented in Appendix C. It should be highlighted that the results are scaled with a factor varying from 7,8 to 13. This is done in order to better understand how the structure reacts to the vibrations.

Table 7.4: Mode shapes of the structure.

Mode shape	Frequency (Hz)
1	100,11
2	100,29
3	100,32
4	393,26
5	393,40
6	397,41
7	420,01
8	420,10
9	476,96
10	511,14

7.6 Buckling analysis

Structural components are often designed to withstand compression loads. In these cases, the service stress may be considerably lower than the yield stress. This is due to a geometric change of the structural part provoking a sudden rise of the bending moment, even when the applied load increases only by small amount.

Considering the example of a beam subjected to a compression force, the straight mean line of the beam evolves to a curved shape, conditioned by the boundary conditions at the beam ends. Under the combined conditions of axial force and bending moment, the relevant deformations are:

$$k_{xx} = \frac{d^2w}{dx^2} \tag{7.8}$$

where, w represents the transverse displacement of the beam of length L, x is the axial coordinate and k_{xx} is the beam curvature. For a material with a Young Modulus E and a section bending moment of inertia I, the internal elastic energy stored in the beam $U_{bending}$ is:

$$U_{bending} = \frac{EI}{2}\int_0^L \left(\frac{d^2w}{dx^2}\right)^2 dx \tag{7.9}$$

By its turn, an axial force F_{ax} performs an external work over an axial displacement u_{ax}. As a result of the beam bending, the projected curve line as a straight line is now smaller than the original length. This work is equal to the internal energy by bending and thus:

$$U_{bending} = \frac{EI}{2}\int_0^L \left(\frac{d^2w}{dx^2}\right)^2 dx = F_{ax} \times u_{ax} \tag{7.10}$$

The axial deformation due to bending buckling distortion is given by:

$$\varepsilon_{ax} = \frac{1}{2}\left(\frac{dw}{dx}^2\right) \tag{7.11}$$

The axial displacement due to buckling, at the end of the veam under the compression force F_{ax} is:

$$u_{ax} = \int_0^L \varepsilon_{ax} dx = \frac{1}{2}\int_0^L \left(\frac{dw}{dx}\right)^2 \tag{7.12}$$

Equaling the internal energy to the work due to the axial compression force:

$$\frac{EI}{2}\int_0^L \left(\frac{d^2w}{dx^2}^2\right) dx = F_{ax}\frac{1}{2}\int_0^L \left(\frac{dw}{dx}\right)^2 dx \tag{7.13}$$

Expressing the displacement w via nodal displacements, under matrix notation, previous expressions can be written as:

$$EI\int_0^L \left([N'']^T[N'']\right) dx\{w_e\} = F_{ax}\int_0^L \left([N']^T[N']\right) dx\{w_e\} \tag{7.14}$$

in which $\{w_e\}$ represents the beam nodal displacement vector and $[N], [N'], [N'']$ represent respectively the shape function matrix and its first and second derivative, for coordinate x along the beam axis.

The previous equation can be rewritten as follows:

$$EI \int_0^L \left([N'']^T [N'']\right) dx\{w_e\} - F_{ax} \int_0^L \left([N']^T [N']\right) dx\{w_e\} = 0 \tag{7.15}$$

Equation 7.15 has only one solution with structural interest that is obtained by prescribing the determinant to zero:

$$Det \left| EI \int_0^L \left([N'']^T [N'']\right) dx - F_{ax} \int_0^L \left([N']^T [N']\right) dx \right| = 0 \tag{7.16}$$

The first element $EI \int_0^L \left([N'']^T [N'']\right) dx$ is the bending stiffness matrix, while the second $F_{ax} \int_0^L \left([N']^T [N']\right) dx$ is the geometric stiffness matrix. For the critical value $F_{ax} = F_crit$, the determinant is zero and the buckling arises.

This is a vital design parameter to check about the bending strength of components subjected to the combination of transverse and compression loads. Thus, a buckling analysis to the structure was made. In Table 7.5 can be seen the 10 load multipliers obtained. None of the load multipliers is inferior to 1, so the structure is not expected to buckle under the load considered in the project. The mode shape are presented in Appendix C.

This buckling analysis, however, is not enough to guarantee the structure's stability. The legs of the lander are the part more prone to buckle and, therefore, an analysis with these bodies must be made.

Table 7.5: Mode shapes of the structure for buckling.

Mode shape	λ_i
1	-16,46
2	-8,05
3	-7,07
4	-6,97
5	-5,91
6	3,04
7	6,88
8	7,01
9	9,09
10	14,37

Chapter 8

Conclusions and future works

The project developed in this dissertation allowed to create a starting point for a propulsion system. However, it is still needed to study in depth the high stresses obtained. Since most appear near sharp edges, a more developed model should be done, rounding them and studying the effect in the results obtained.

Regarding the project, in order to overcome the high stresses in the ear of the hexagons of the cage, it would be useful to study how much it could be reduced by increasing the thickness of the ear and therefore the area of contact. Another option would be to change the design of the hexagons, since the lander is modular. Furthermore, the weight of the batteries, that is not considered in the project, may enable to reduce the weight of the ballast weights, and therefore, reduce the high stresses generated in the ears of the hexagon.

Regarding the high stresses presented in the other pieces, they could also be overcome by developing a solution similar to the sketch represented in Figure 6.6 d), one of the presented in the design process, since most of them are related to the load along the Z axis and the lack of rigidity of the mounting along this axis.

Even though that the results obtained suggest that the project cannot be done as is, the solutions proposed might enable it. Nevertheless, this project is a useful model for a starting point for a propulsion system. The simplicity of the pieces projected, as well as their doable production are a key aspect that will certainly be useful to future projects.

In order to complement this project, it is still needed to analyse the buckling behavior of the whole structure, including the legs of the lander, that are the critical parts of the vehicle. It is also needed to calculate the batteries required for the operation of the vehicle, as well as conclude the detaching system for the ballast weights.

The high cost of the thrusters presents an evident impediment on the development of the project. It should be a priority to search for cheaper thrusters. It should also be considered and studied the alternative of developing a VBS that would allow the lander to move vertically. The power required for the thrusters would be much inferior to the one considered in the project and it would not be necessary to use ballast weights. In this case, the model developed could still be helpful for the thrusters that would be needed to move in the horizontal direction.

In spite of this, thanks to the recent trend of electric vehicles, it is expected that both batteries and electric motors' prices drop and capacities rise, as research develops. So, it is probable that in the future, there will be available better thrusters and at lower prices, meaning that the concept of this project may become more realistic.

Appendix A

Bolt and washer’s calculations

Dimensioning of the screws

Considering M14 stainless steel screws, with the properties:

$A_t := 115 \cdot mm^2$ Tensile area [56]

$d_n \equiv 14\ mm$ Nominal diameter [57]

$d_h := 21\ mm$ Head diameter [57]

$A_h := \frac{\pi}{4} \cdot \left(d_h^{\,2} - d_n^{\,2}\right) = 192.423\ mm^2$ Area of contact

Yield strength S_y for staineless steel, varies from 257 to 1140 MPa [40]. Due to the high difference,it was considered that the S_y of the stainless steel used in the project would be 1.5 times higher than the minimum. Thus:

$S_y \equiv 1.5 \cdot 257\ MPa = 385.5\ MPa$

Case 1 - for the two screws in the image:

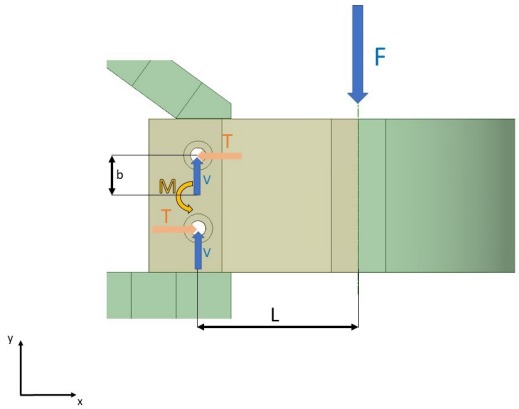

$b := 20 \cdot mm$
$L := 174\ mm$
$F := -4417.2\ N$

$V := \frac{-F}{2} = \left(2.209 \cdot 10^3\right)\ N$

$M := L \cdot F = -768.593\ N \cdot m$

In each bolt:

$V = \left(2.209 \cdot 10^3\right)\ N$

$T := \frac{M}{2 \cdot b} = -1.921 \cdot 10^4\ N$

$F_R := \sqrt[2]{T^2 + \left(\frac{V}{2}\right)^2} = \left(1.925 \cdot 10^4\right)\ N$

Length of the bolt

$t \equiv 90\ mm$ Thickness of the connected parts

$h_{nut} \equiv 12.8\ mm$ Height of the nut [57]

$l := t + h_{nut} + 2\ mm + 2\ mm = 106.8\ mm$ Length of the bolt

Considering:

2 mm for a washer
2 mm for 2 threads beyond the nut

Accordingly to Simões Morais [57], the closest standard value, higher than 106.8 is

$l := 110\ mm$

The threaded length can be calculated through

$l_t := 2 \cdot d_n + 6\ mm = 34\ mm$

Thus, the unthreaded part is

$l_u := l - l_t = 76\ mm$

The unthreaded portion will be smaller than the thickness, so the bolt will tend to shear across its minor diameter.

$A_s := 104 \cdot mm^2$ Value obtained in [56]

Finnaly, it is possible to obtain the shear stress acting in the screw

$$S_{screw} := \frac{F_R}{A_s} = 185.063\ MPa$$

The shear strength S_s can be approximated through [56]:

$S_s := 0.6 \cdot S_y = 231.3\ MPa$

$\frac{S_{screw}}{S_s} = 0.8$ Tension in each screw, inferior to S_s

Case 2 - for the 4 bolts represented in the image:

Considering M10 bolts

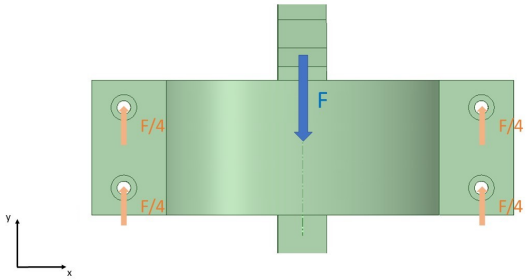

$F := -4417.3 \cdot N$ Force caused by the thruster

$F_{screw} := -\frac{F}{4} = (1.104 \cdot 10^3)\ N$ Force that actuates in each screw

$d_{n\_2} \equiv 10\ mm$

Length of the bolt

$t_2 \equiv 30\ mm$ Thickness of the connected parts

$h_{nut\_2} \equiv 12.8\ mm$ Height of the nut

$l := t_2 + h_{nut\_2} + 2\ mm + 2\ mm = 46.8\ mm$ Length of the bolt

Considering:

2 mm for a washer
2 mm for 2 threads beyond the nut

Accordingly to Simões Morais [57], the closest standardized value, higher than 46.8 mm is

$l_2 := 50\ mm$

The threaded length can be calculted through

$l_{t\_2} \equiv 2 \cdot d_{n\_2} + 6\ mm = 26\ mm$

Thus, the unthreaded part is

$l_{u\_2} := l_2 - l_{t\_2} = 24\ mm$

The unthreaded portion will be smaller than the thickness, so the bolt will tend to shear across its minor diameter.

$A_{s\_2} := 52.3 \cdot mm^2$ Value obtained in [56]

Finnaly, it is possible to obtain the shear stress acting in the screw

$$S_{screw} := \frac{F_{screw}}{A_{s\_2}} = 21.115\ MPa$$

$$\frac{S_{screw}}{S_s} = 0.091$$

Tension in each screw, inferior to S_s

Pre-tension

For nonpermanent connections [56]:

$$F_i = 0.75 \cdot F_p$$

Where:

F_i represents pre-tension
F_p represents the proof load

F_p can be obtained through [56]

$$F_p = A_t \cdot S_p$$

And S_p can be approximated through [56]

$$S_p = 0.85\ S_y$$

So, and since it is a nonpermanent connection, for M14

$$S_y = 385.5\ \boldsymbol{MPa}$$

$$S_p := 0.85 \cdot S_y = 327.675\ \boldsymbol{MPa}$$

$$F_p := A_t \cdot S_p = \left(3.768 \cdot 10^4\right)\ \boldsymbol{N}$$

$$F_i := 0.75 \cdot F_p = \left(2.826 \cdot 10^4\right)\ \boldsymbol{N}$$ Maximum value for pre-tension

Effect of pre-tension on POM

$$A_h := \frac{\pi}{4} \cdot \left({d_h}^2 - {d_n}^2\right) = 192.423\ \boldsymbol{mm}^2$$ Area of contact

$$S_{POM} := \frac{F_i}{A_h} = 146.875\ \boldsymbol{MPa}$$ Stress caused in POM

The compressive strength, σ_c, of POM is 72 MPa. For security, it will be considered as 0,7 of that value.

$$\sigma_c \equiv 0.7 \cdot 72\ \boldsymbol{MPa} = 50.4\ \boldsymbol{MPa}$$

Therefore, the stress caused in POM is higher than the compressive strength allowed. In order to solve this, a washer will be dimensioned.

Washer dimensioning

The diameter of the washer , d_w, can be obtained by multiplying the area of contact by the stress caused in POM, S_{POM}, and dividing by the area of the washer. This value must be lower than the compressive strength of the POM, σ_c .

$$\frac{S_{POM} \cdot A_h}{\frac{\pi}{4}\left(d_w{}^2 - d_n{}^2\right)} = \sigma_c$$

$$d_w := \sqrt[2]{\frac{S_{POM} \cdot A_h}{\frac{\pi}{4} \cdot \sigma_c} + d_n{}^2} = 30.166\ mm$$

The diameter of the washer must be superior to d_w

Accordingly to Simões Morais [57], for M14, the closest standard diameter for a washer is 44mm.

For the M10 bolts

Repeating the same process:

$A_{t\_3} := 58 \cdot mm^2$ Tensile area

$d_{n\_3} \equiv 8\ mm$ Nominal diameter

$d_{h\_3} := 16\ mm$ Head diameter

$A_{h\_3} := \frac{\pi}{4} \cdot \left(d_{h\_3}{}^2 - d_{n\_3}{}^2\right) = 150.796\ mm^2$ Area of contact

$S_y = 385.5\ MPa$

$S_p := 0.85 \cdot S_y = 327.675\ MPa$

$F_p := A_{t\_3} \cdot S_p = \left(1.901 \cdot 10^4\right)\ N$

$F_i := 0.75 \cdot F_p = \left(1.425 \cdot 10^4\right)\ N$ Maximum value for pre-tension

Effect of pre-tension on POM

$$S_{POM} := \frac{F_i}{A_{h\_3}} = 94.524\ MPa$$ Stress caused in POM

The compressive strength, σ_c, of POM is 72 MPa. For security, it will be considered as 0,7 of that value.

$$\sigma_{c\_3} \equiv 0.7 \cdot 72\ MPa = 50.4\ MPa$$

Therefore, the stress caused in POM is higher than the compressive strength allowed. In order to solve this, a washer will be dimensioned.

Washer dimensioning

The diameter of the washer , d_w, can be obtained by multiplying the area of contact by the stress caused in POM, S_{POM}, and dividing by the area of the washer. This value must be lower than the compressive strength of the POM, σ_c .

$$\frac{S_{POM} \cdot A_{h\_3}}{\frac{\pi}{4}\left({d_{w\_3}}^2 - {d_{n\_3}}^2\right)} = \sigma_{c\_3}$$

$$d_{w\_3} := \sqrt[2]{\frac{S_{POM} \cdot A_{h\_3}}{\frac{\pi}{4} \cdot \sigma_{c\_3}} + {d_{n\_3}}^2} = 20.593\ mm$$

The diameter of the washer must be superior to d_{w_3}

Accordingly to Simões Morais [57], for M10, the closest standard diameter for a washer is 30mm.

Appendix B

Technical drawings

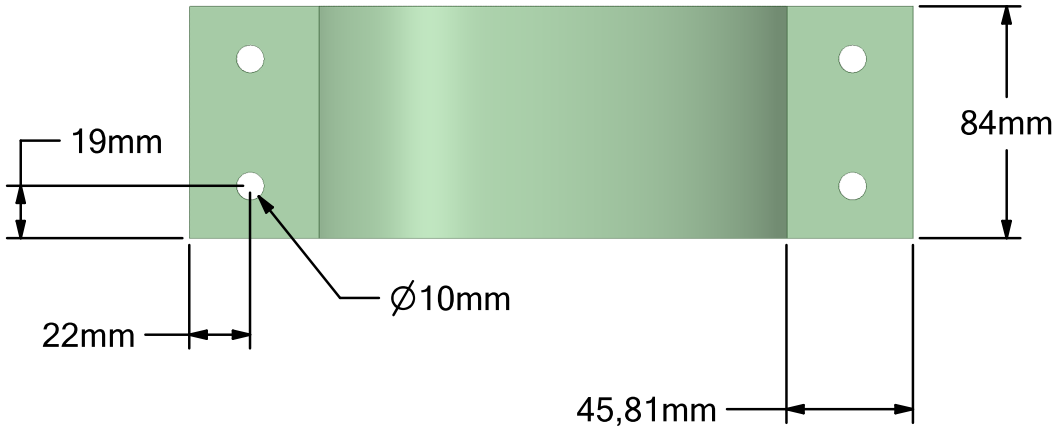

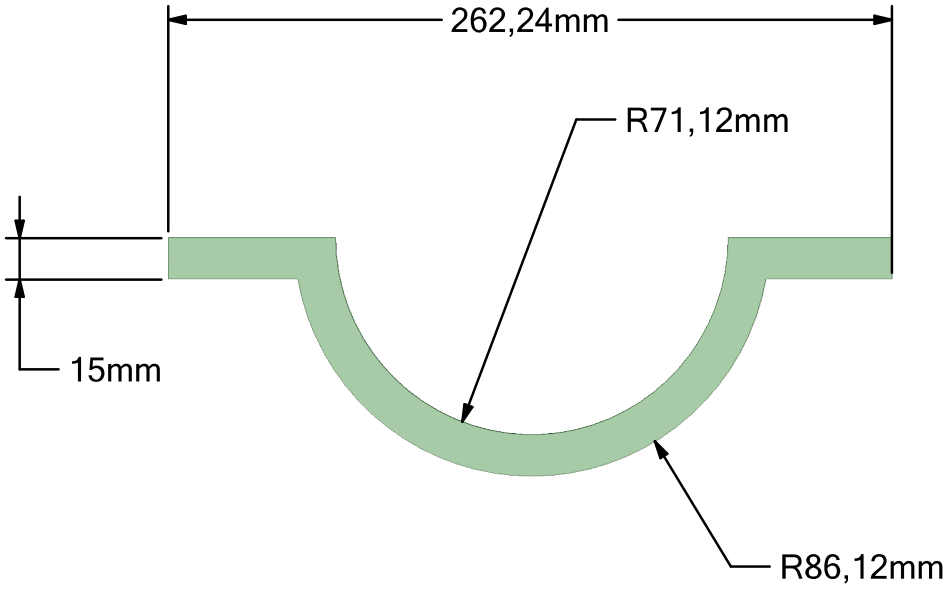

SIZE	CAGE CODE	DWG NO.	REV
A4			
SCALE 2:5			SHEET 1 of 6

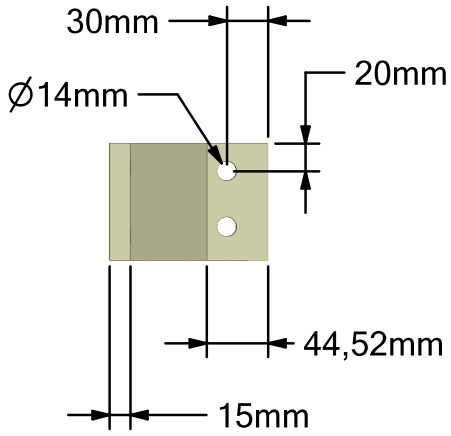

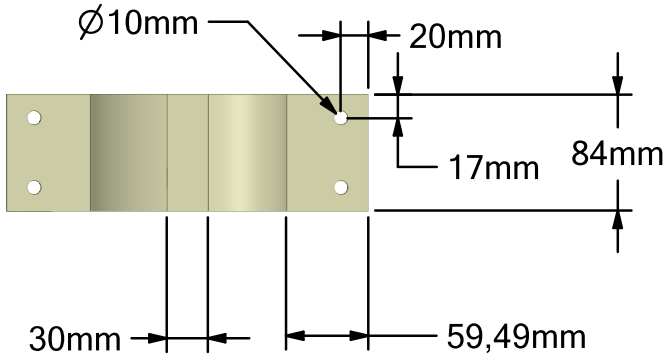

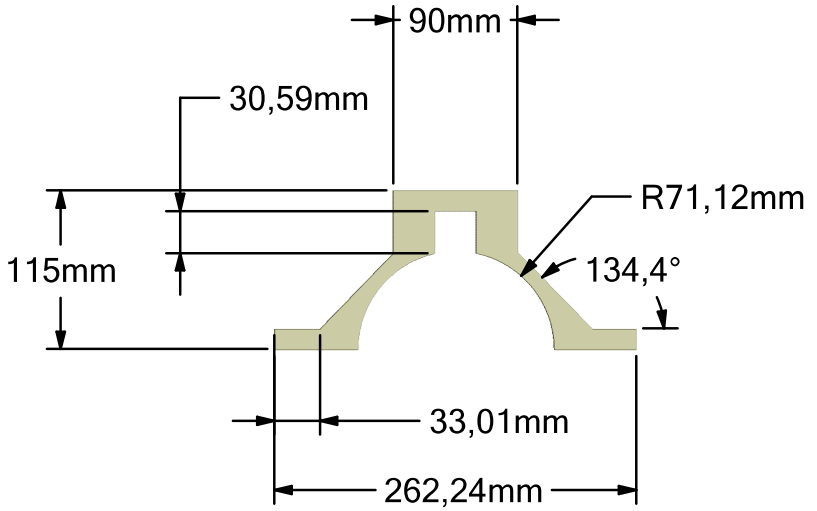

SIZE A4	CAGE CODE	DWG NO.	REV
SCALE 1:5			SHEET 2 of 6

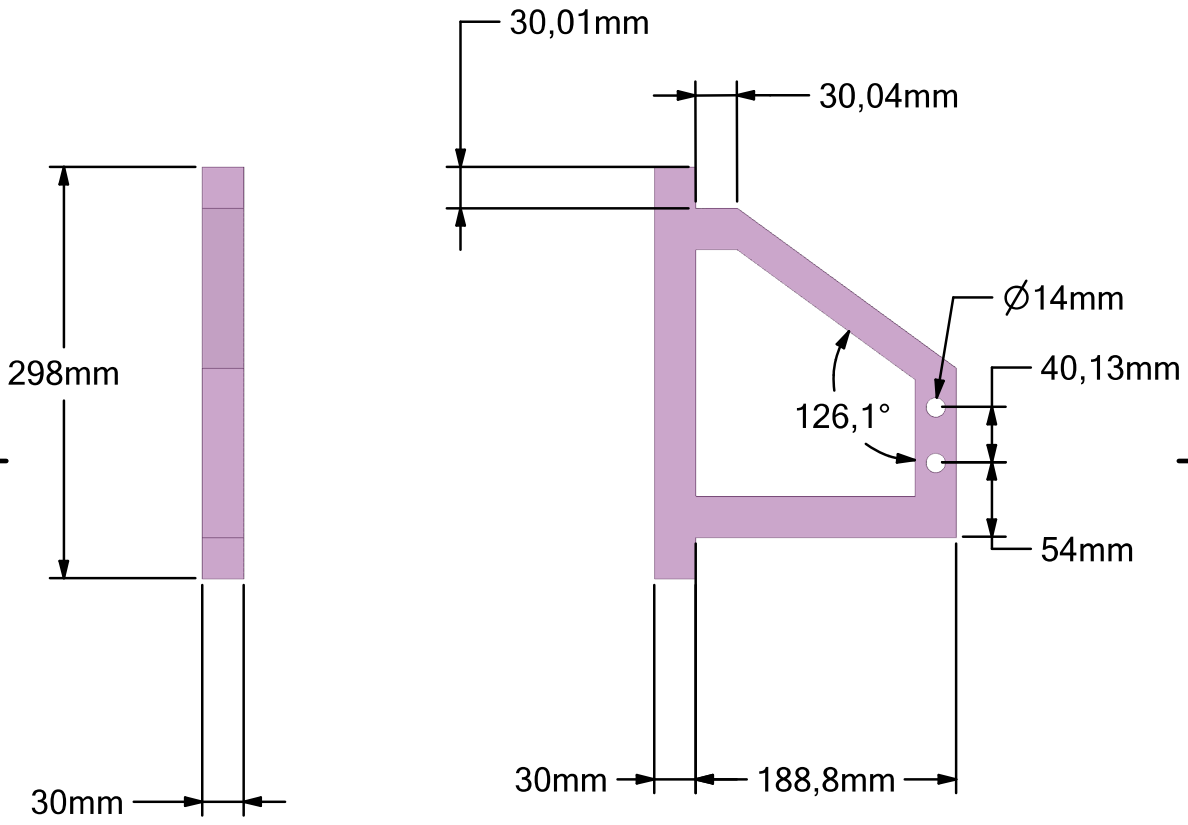

SIZE	CAGE CODE	DWG NO.	REV
A4			
SCALE 1:5			SHEET 3 of 6

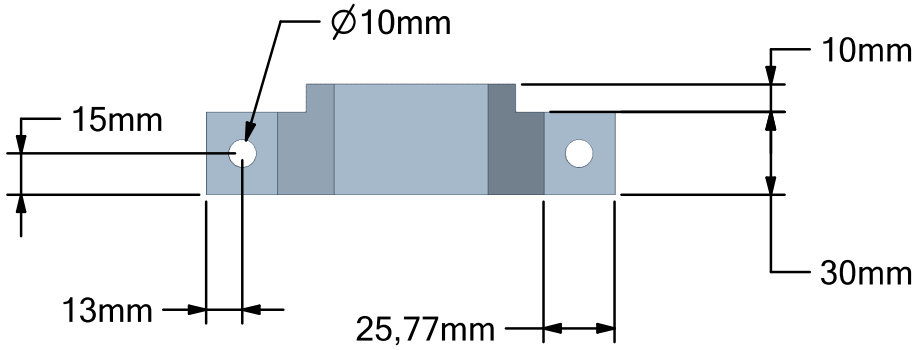

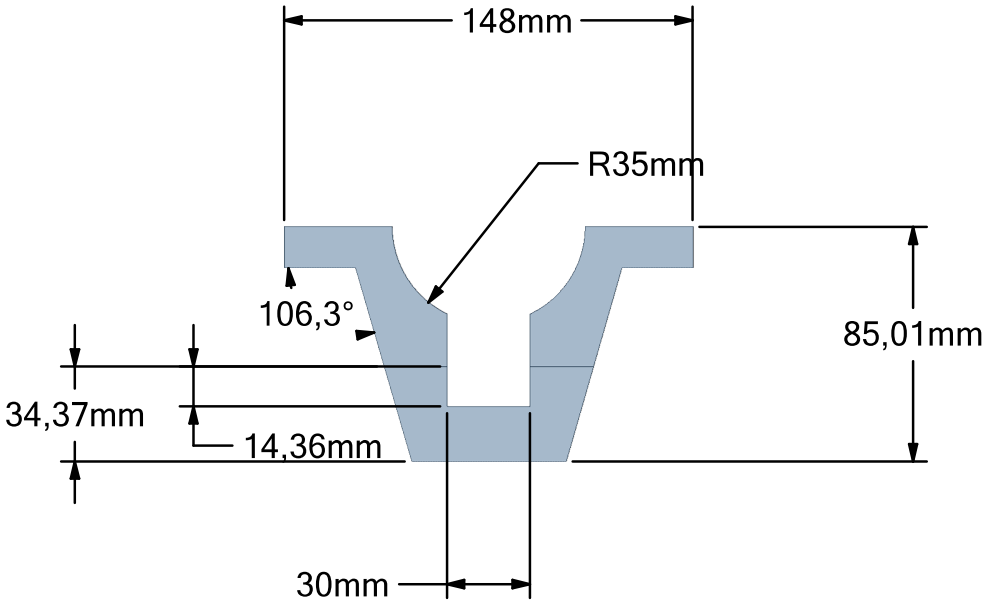

SIZE	CAGE CODE	DWG NO.	REV
A4			
SCALE 2:5			SHEET 4 of 6

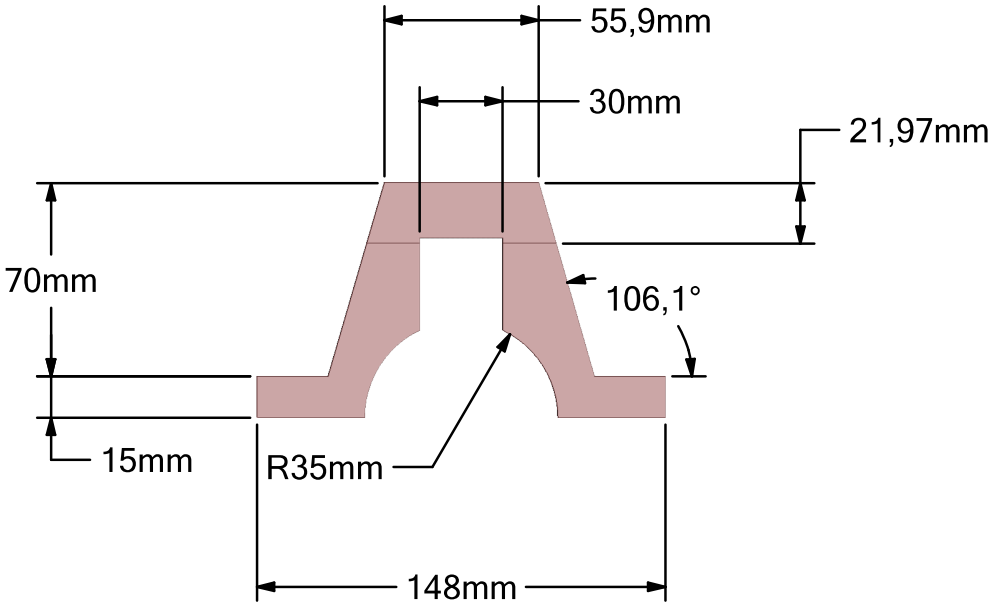

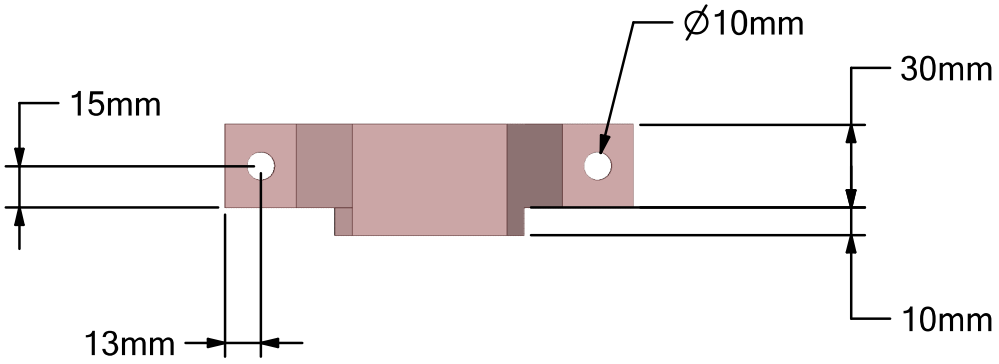

SIZE A4	CAGE CODE	DWG NO.	REV
SCALE 2:5			SHEET 5 of 6

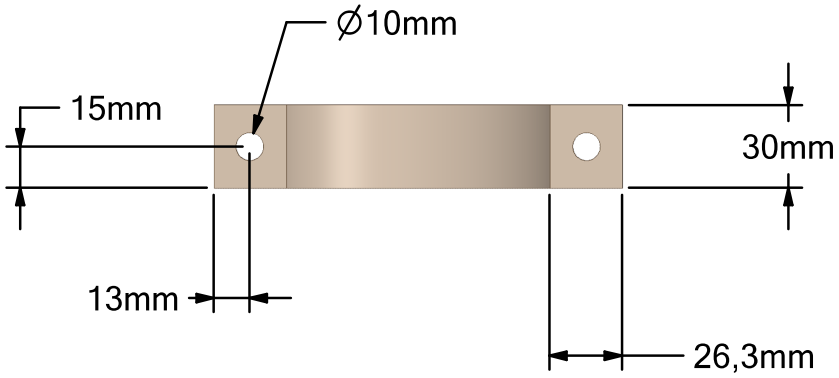

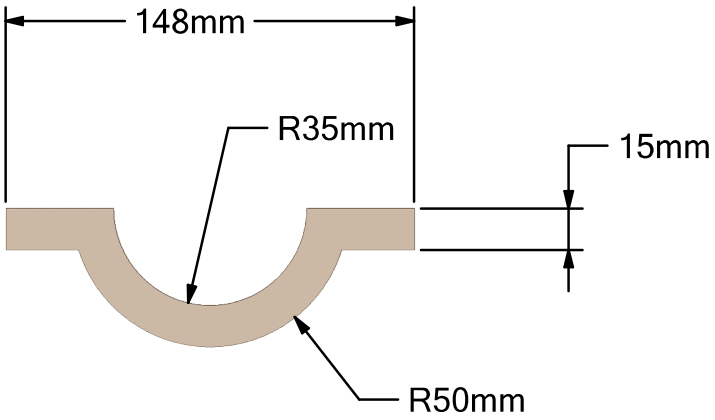

SIZE A4	CAGE CODE	DWG NO.	REV
SCALE 2:5			SHEET 6 of 6

Appendix C

Mode shapes of modal and buckling analysis

C.1 Modal analysis

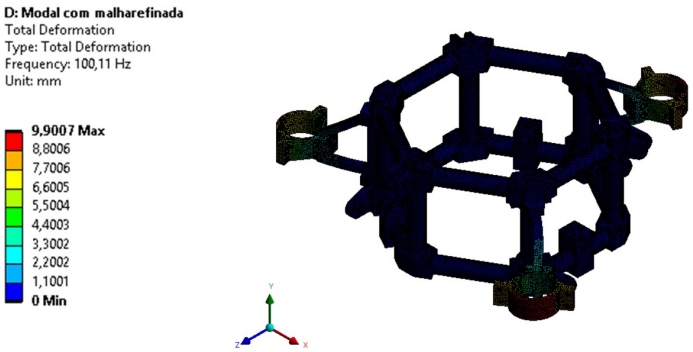

Figure C.1: Mode shape 1.

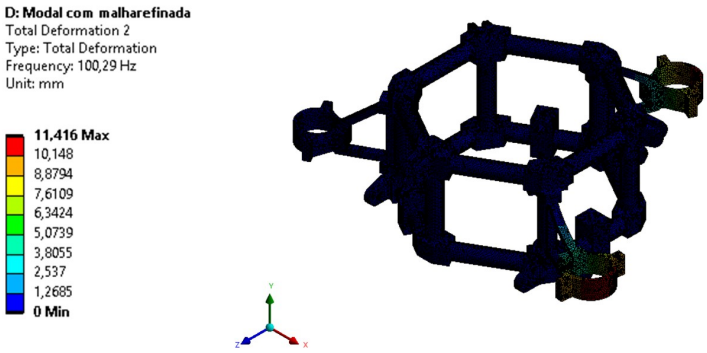

Figure C.2: Mode shape 2.

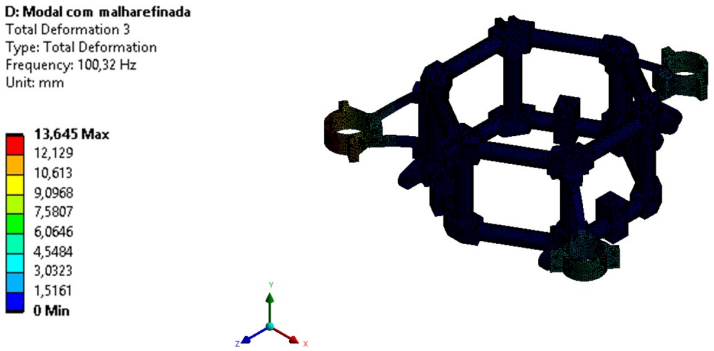

Figure C.3: Mode shape 3.

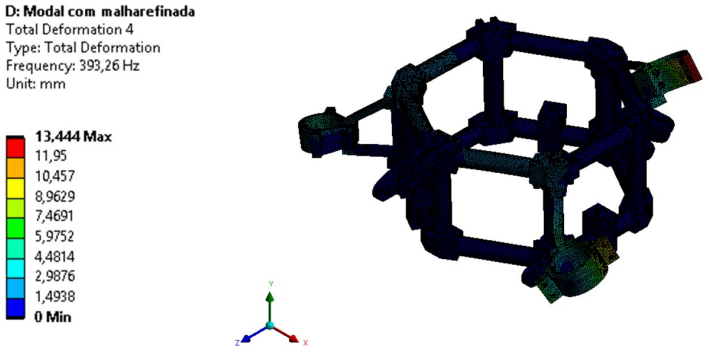

Figure C.4: Mode shape 4

.

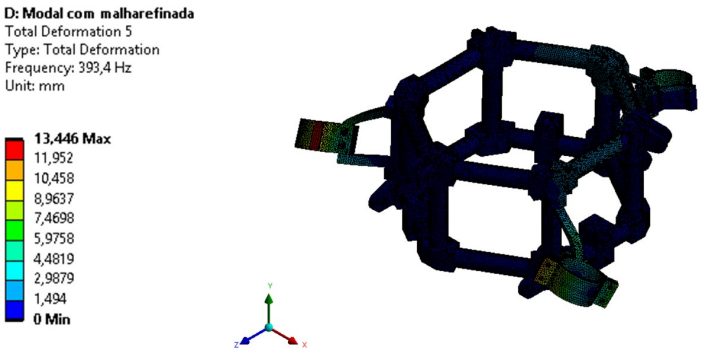

Figure C.5: Mode shape 5.

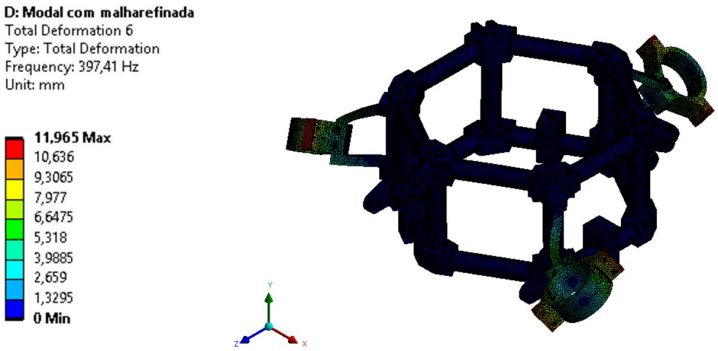

Figure C.6: Mode shape 6.

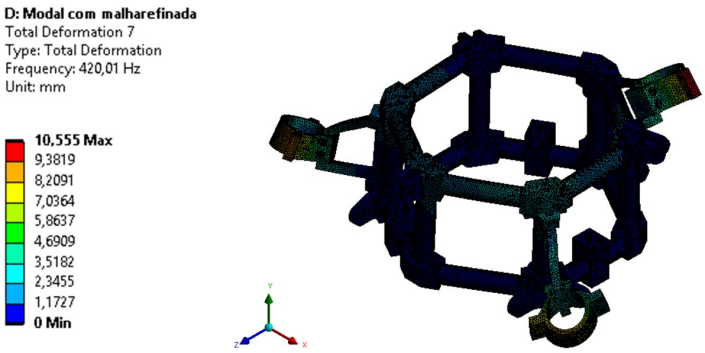

Figure C.7: Mode shape 7.

.

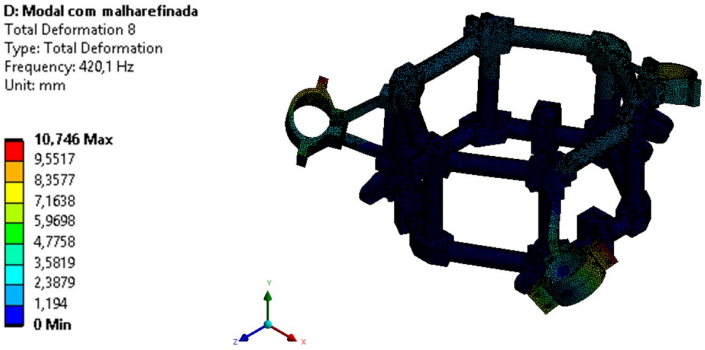

Figure C.8: Mode shape 8.

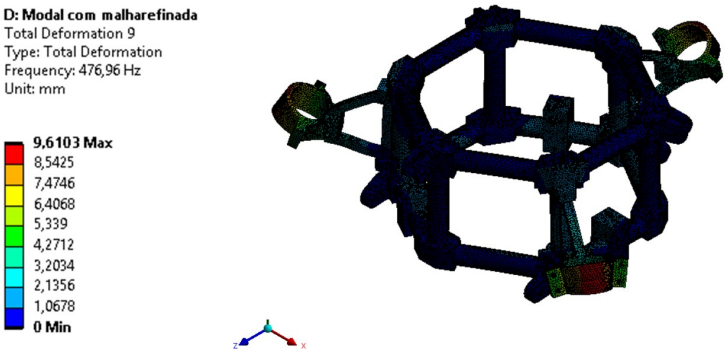

Figure C.9: Mode shape 9.

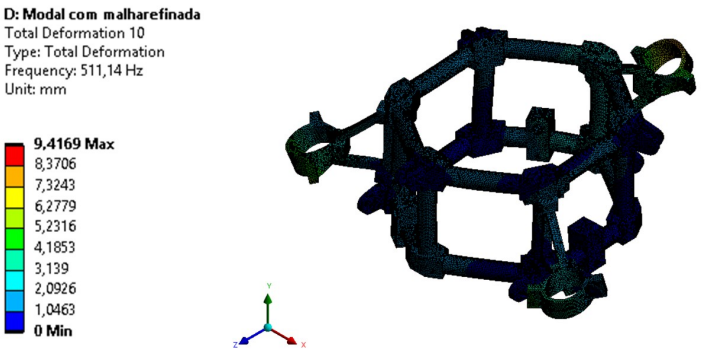

Figure C.10: Mode shape 10.

.

C.2 Buckling analysis

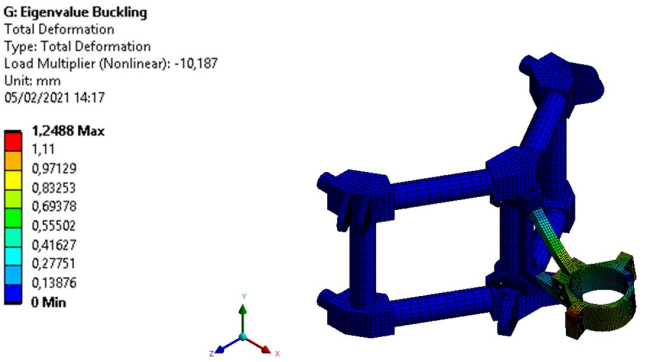

Figure C.11: Mode shape 1.

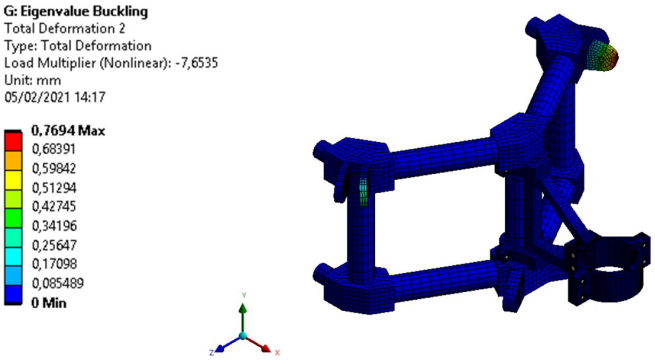

Figure C.12: Mode shape 2.

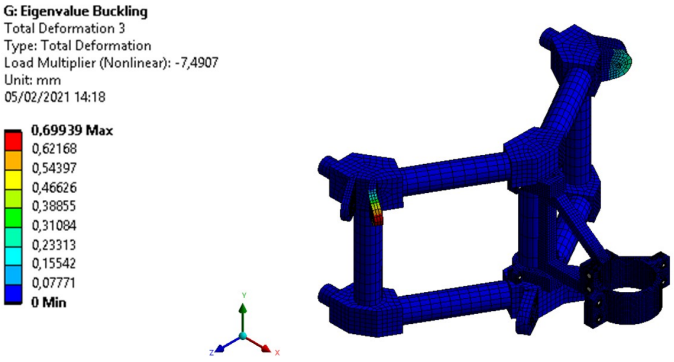

Figure C.13: Mode shape 3.

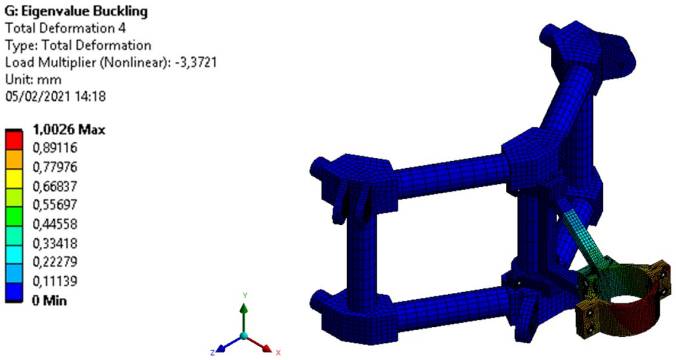

Figure C.14: Mode shape 4.

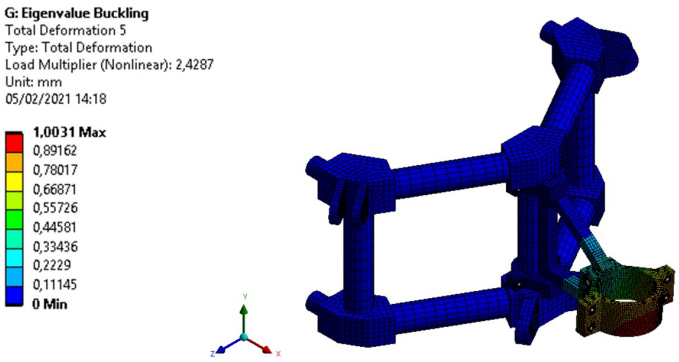

Figure C.15: Mode shape 5.

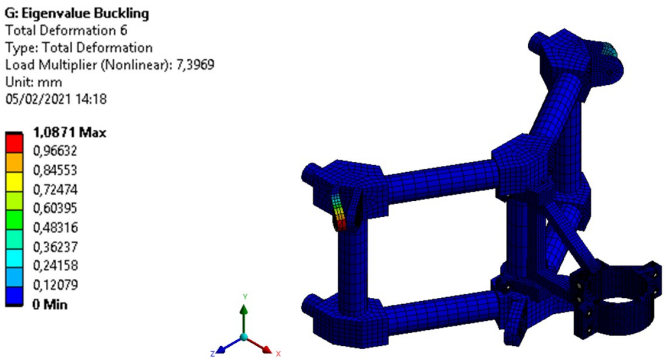

Figure C.16: Mode shape 6.

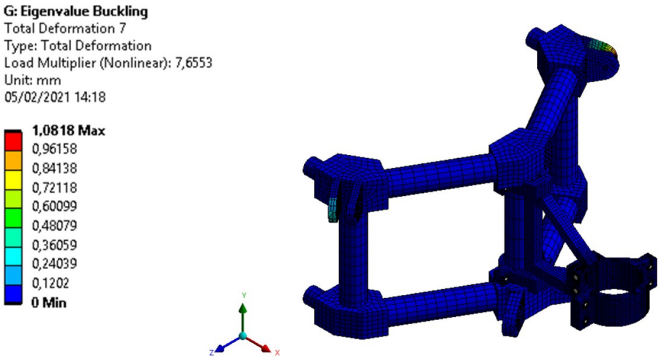

Figure C.17: Mode shape 7.

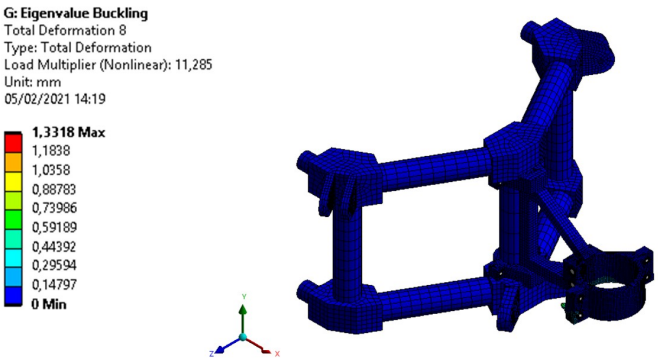

Figure C.18: Mode shape 8.

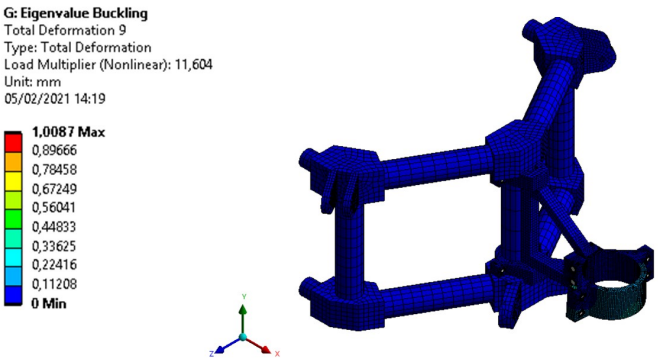

Figure C.19: Mode shape 9.

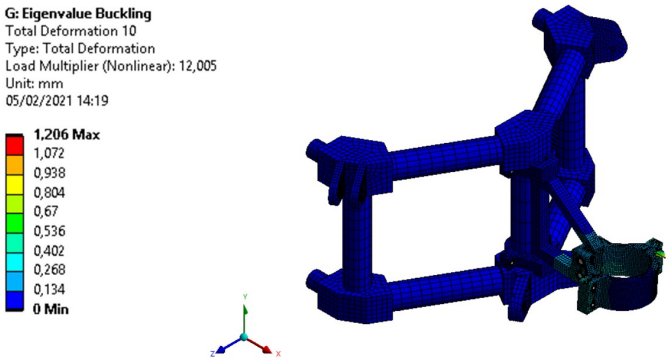

Figure C.20: Mode shape 10.

Appendix D

Data about the chosen thruster

Model 8020 Thruster
Input Power & Thrust vs. Propeller RPM

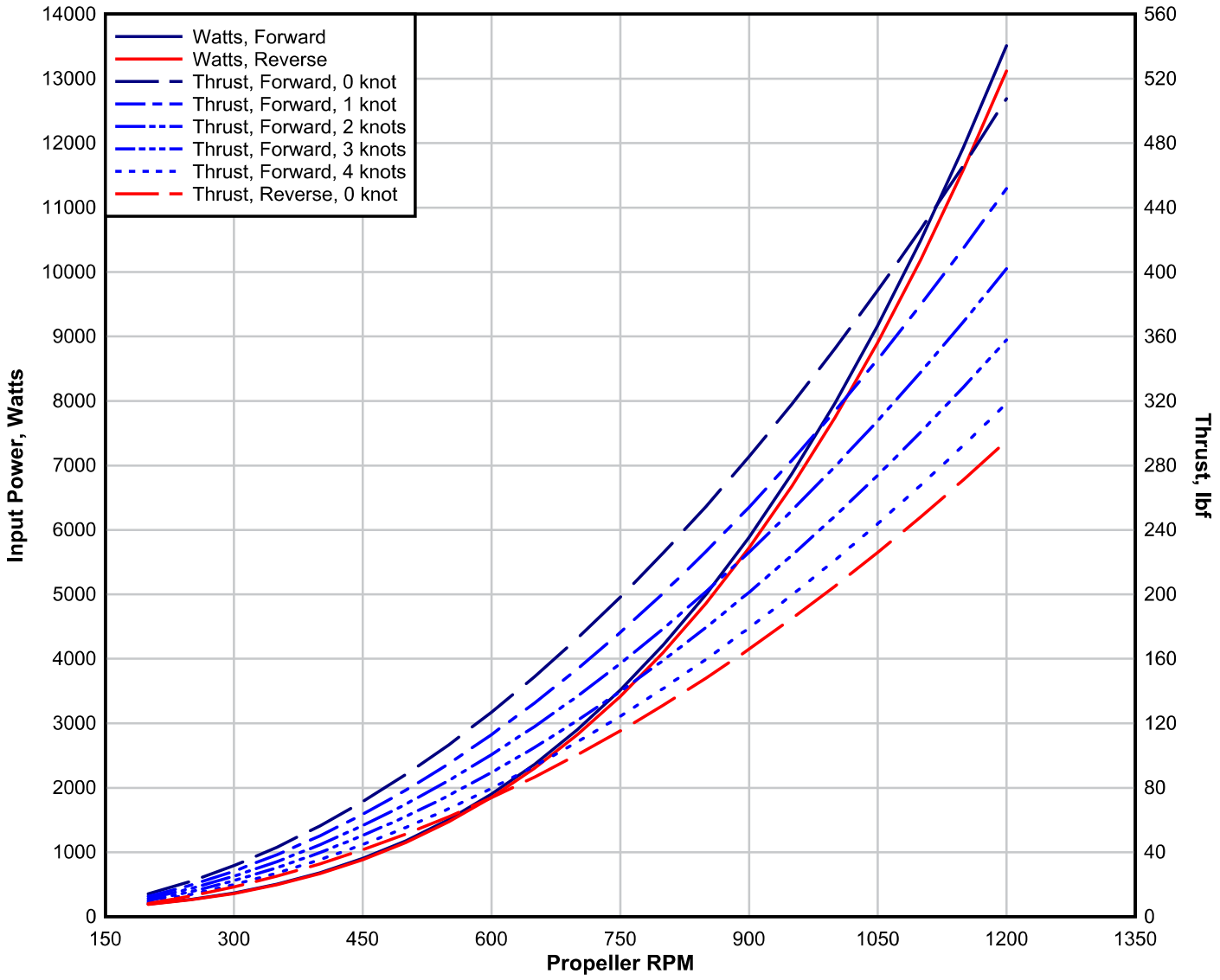

Model 8020 Thruster
Thrust vs. Voltage Change

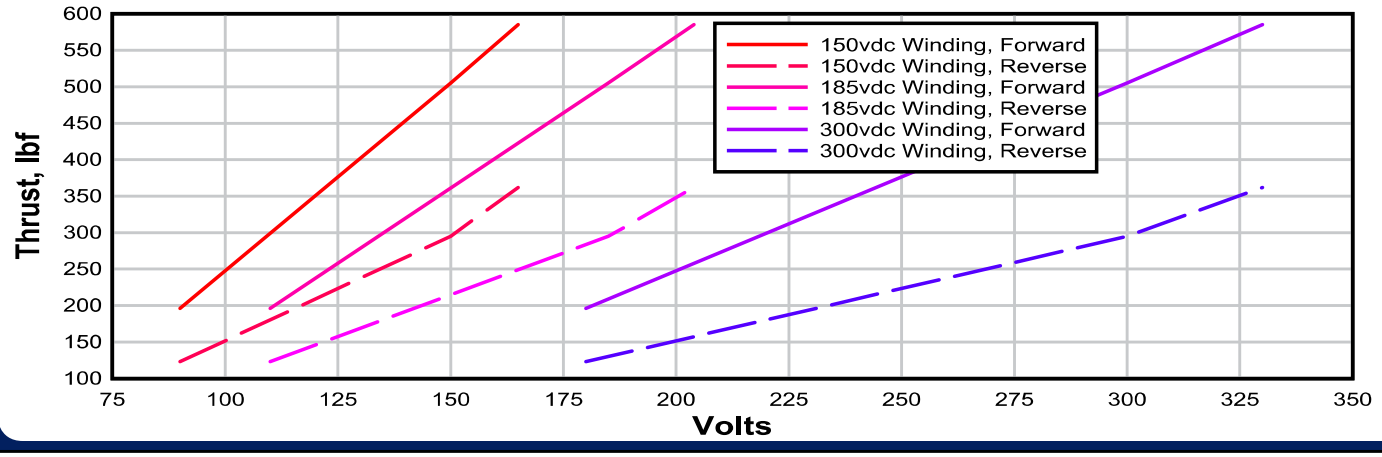

Bibliography

[1] P. Oceonography, "Why the Oceans are Important !," *Project Oceanography*, vol. 1, no. June, 1998.

[2] C. Suisse, "The Tides Are Turning: Why the Blue Economy Matters." [Online]. Available: https://www.credit-suisse.com/about-us-news/en/articles/news-and-expertise/the-tides-are-turning-why-the-blue-economy-matters-201806.html [Accessed Feb. 13, 2020].

[3] European Comission, "The EU Blue Economy Report 2020," tech. rep., European Comission, 2020.

[4] Sea Around Us, "Sea Around Us." [Online]. Available: http://www.seaaroundus.org/data/#/ [Accessed Oct. 09, 2020].

[5] European Comission, "Blue Indicators Online Dashboard." [Online]. Available: https://blueindicators.ec.europa.eu/access-online-dashboard_en [Accessed Oct. 09, 2020], 2020.

[6] A. M. Helmenstine, "Deep Sea Exploration History and Technology." [Online]. Available: https://www.thoughtco.com/deep-sea-exploration-4161315 [Accessed Mar. 08, 2020], 2020.

[7] N. O. Association and Atmospheric, "How much of the ocean have we explored?." [Online]. Available: https://oceanservice.noaa.gov/facts/exploration.html [Accessed Feb. 13, 2020], 2018.

[8] S. Katsanevakis, I. Wallentinus, A. Zenetos, E. Leppäkoski, M. E. Çinar, B. Oztürk, M. Grabowski, D. Golani, and A. C. Cardoso, "Impacts of invasive alien marine species on ecosystem services and biodiversity: A pan-European review," *Aquatic Invasions*, vol. 9, no. 4, pp. 391–423, 2014.

[9] A. University, "Macroalgae: A New Source of Bio-Based Products." [Online]. Available: https://stateofgreen.com/en/partners/aarhus-university/solutions/macroalgae-as-a-new-source-of-bio-based-products/ [Accessed Feb. 13, 2020], 2020.

[10] W. O. Initiative, "Our Ocean conference generates pledges worth US$64bn." [Online]. Available: https://www.woi.economist.com/our-ocean-conference-generates-pledges-worth-us64bn/ [Accessed Apr. 06, 2020], 2019.

[11] R. D. Christ and R. L. Wernli, *Thrusters*. Elsevier Ltd, 2014.

[12] Deep Trekker, "What Are Underwater ROVs & What Are They Used For?." [Online]. Available: https://www.deeptrekker.com/resources/underwater-rovs [Accessed Jun. 03, 2020], 2020.

[13] Fugro, "ROV - Capabilities." [Online]. Available: https://www.fugro.com/our-services/marine-asset-integrity/rov-services-and-tooling/rov-remote-operated-vehicles#!%7Ctabbed1 [Accessed Mar. 26, 2020], 2020.

[14] T. Salgado-Jimenez, J. L. Gonzalez-Lopez, L. F. Martinez-Soto, E. Olguin-Lopez, P. A. Resendiz-Gonzalez, and M. Bandala-Sanchez, "Deep water ROV design for the Mexican oil industry," *OCEANS'10 IEEE Sydney, OCEANSSYD 2010*, pp. 1–6, 2010.

[15] URI, "Ocean and space exploration blend at URI's Graduate School of Oceanography." [Online]. Available: https://today.uri.edu/news/ocean-and-space-exploration-blend-at-uris-graduate-school-of-oceanography/ [Accessed Mar. 17, 2020], 2019.

[16] Blue Robotics, "BlueROV2." [Online]. Available: https://bluerobotics.com/store/rov/bluerov2/ [Accessed Mar. 18, 2020], 2020.

[17] Nautilus Live, "ROV Hercules." [Online]. Available: https://nautiluslive.org/tech/rov-hercules [Accessed Mar. 04, 2020], 2020.

[18] Geomar, "ROV KIEL 6000 - Technical Specifications - Overview." [Online]. Available: https://www.geomar.de/en/centre/central-facilities/tlz/rovkiel6000/specifications-logistics/ [Accessed Mar. 18, 2020], 2020.

[19] R. B. Wynn, V. A. Huvenne, T. P. Le Bas, B. J. Murton, D. P. Connelly, B. J. Bett, H. A. Ruhl, K. J. Morris, J. Peakall, D. R. Parsons, E. J. Sumner, S. E. Darby, R. M. Dorrell, and J. E. Hunt, "Autonomous Underwater Vehicles (AUVs): Their past, present and future contributions to the advancement of marine geoscience," *Marine Geology*, vol. 352, pp. 451–468, 2014.

[20] F. Aguirre, S. Vargas, D. Valdés, and J. Tornero, "State of the Art of Parameters for Mechanical Design of an Autonomous Underwater Vehicle," *International Journal of Oceans and Oceanography ISSN*, vol. 11, no. 1, pp. 973–2667, 2017.

[21] K. Jerosch, M. Schlüter, and R. Pesch, "Spatial analysis of marine categorical information using indicator kriging applied to georeferenced video mosaics of the deep-sea Håkon Mosby Mud Volcano," *Ecological Informatics*, vol. 1, no. 4, pp. 391–406, 2006.

[22] V. P. Shah, "Design considerations for engineering autonomous underwater vehicles," *Design considerations for engineering autonomous underwater vehicles*, 2007.

[23] Woods Hole Oceanographic Institution, "R.I.P. A.B.E : Woods Hole Oceanographic Institution." [Online]. Available: https://www.whoi.edu/page.do?pid=7150&tid=282&cid=70906 [Accessed Mar. 18, 2020], 2020.

[24] M. Airhart, "DEPTHX AUV." [Online]. Available: https://en.wikipedia.org/wiki/DEPTHX [Accessed Mar. 17, 2020], 2020.

[25] AUVAC, "Explore Database." [Online]. Available: https://auvac.org/explore-database/ [Accessed Mar. 20, 2020], 2020.

[26] X. Xiang, Z. Niu, L. Lapierre, and M. Zuo, "Hybrid underwater robotic vehicles: The state-of-the-art and future trends," *HKIE Transactions Hong Kong Institution of Engineers*, vol. 22, no. 2, pp. 103–116, 2015.

[27] Snipview, "Nereus - underwater vehicle." [Online]. Available: https://www.snipview.com/q/nereus_(underwater_vehicle) [Accessed Mar. 17, 2020], 2020.

[28] Blue Zone Group, "Versatile Double Eagle Integrates Solstice Sonar." [Online]. Available: https://www.bluezonegroup.com.au/announcements/versatile-double-eagle-integrates-solstice-sonar [Accessed Apr. 21, 2020], 2019.

[29] SAAB, "Double Eagle SAROV - One system, multiple functions," *SAAB Technology*, p. 4, 2019.

[30] SRS, "Fusion datasheet," *Strategic Robotic Systems*, p. 2, 2019.

[31] A. D. Bowen, D. R. Yoerger, C. Taylor, R. McCabe, J. Howland, D. Gomez-Ibanez, J. C. Kinsey, M. Heintz, G. McDonald, D. Peters, C. Young, J. Buescher, B. Fletcher, L. L. Whitcomb, S. C. Martin, S. E. Webster, and M. Jakuba, "The Nereus hybrid underwater robotic vehicle," *Underwater Technology*, vol. 28, no. 3, pp. 79–89, 2009.

[32] A. et all TENGBERG, "Benthic chamber and profiling landers in oceanography - A review of design, technical solutions and functioning," tech. rep., Elsevier Science, 1995.

[33] K. S. Black, G. R. Fones, O. C. Peppe, H. A. Kennedy, and I. Bentaleb, "An autonomous benthic lander: Preliminary observations from the UK BENBO thematic programme," *Continental Shelf Research*, vol. 21, no. 8-10, pp. 859–877, 2001.

[34] J. L. Watson and B. E. Huntington, "Assessing the performance of a cost-effective video lander for estimating relative abundance and diversity of nearshore fish assemblages," *Journal of Experimental Marine Biology and Ecology*, vol. 483, pp. 104–111, 2016.

[35] J. Chen, Q. Zhang, A. Zhang, L. He, and Q. Chen, "Sea trial and free-fall hydrodynamic research of a 7000-meter lander," *OCEANS 2015 - MTS/IEEE Washington*, pp. 1–5, 2016.

[36] J. Pedro, N. Mathias, R. Hoveling, H. Alves, and T. Morais, "An innovative benthic lander for macroalgae monitoring in shallow-water environments," 2019.

[37] Ecogig, "Systems & Sensors." [Online]. Available: https://ecogig.org/systems-and-sensors [Accessed Mar. 17, 2020], 2020.

[38] Kongsberg Group, "K-Lander Autonomous Seabed Sensor Carrier," *Kongsberg*, vol. 1, no. March, 2015.

[39] Oregon Marine Reserves, "New Marine Reserves Publication." [Online]. Available: https://oregonmarinereserves.com/2016/07/21/publication/ [Accessed Mar. 23, 2020], 2016.

[40] Edupack, "CES EduPack," 2020.

[41] T. Hyakudome, "Design of Autonomous Underwater Vehicle," Tech. Rep. 1, JAMSTEC, 2011.

[42] E. Oñate, *Structural Analysis with the Finite Element Method - Linear Statics - Volume 1 - Basis and Solids*. Springer, 1st ed., 2009.

[43] F. et al. Gonçalves, "Numerical modelling of full-scale subsea lander AMALIA with in-situ conditions.".

[44] W. Munson, Bruce; Young, Donald; Okiishi, Theodore; Huebsch, *Fundamentals of fluid mechanics*. Don Fowley, 6th ed., 2009.

[45] H. Franklin, *Variable Buoyancy System Metric*. PhD thesis, MIT, 2009.

[46] A. Z. T. A. H. Sylvester, J. A. Delmerico and B. S. Bingham, "Variable buoyancy control for a bottom skimming autonomous underwater vehicle," vol. 2014 Ocean, pp. 1–6, 2014.

[47] C. Thompson, "A conceptual design study of a hovering system controller for an Autonomous Underwater Vehicle," *Mechanical engineering*, 1987.

[48] Technadyne, "Installation & Mounting of Tecnadyne Dc Brushless Thrusters," *Technadyne application note*, 2006.

[49] W. Wang, R. Engelaar, X. Chen, and J. Chase, "The State-of-Art of Underwater Vehicles - Theories and Applications," *Mobile Robots - State of the Art in Land, Sea, Air, and Collaborative Missions*, no. May, 2009.

[50] Vision Aerial, "Switch blade elite." [Online]. Available: https://www.visionaerial.com/platforms/switchblade#overview [Accessed Oct. 10, 2020], 2020.

[51] DJI, "DJI Matrice 600 PRO." [Online]. Available: https://www.dji.com/pt/matrice600-pro/info#specs [Accessed Oct. 09, 2020], 2020.

[52] "Tecnadyne - Products." [Online]. Available: https://tecnadyne.com/products [Accessed Jun. 05, 2020].

[53] "Copenhagen Subsea." [Online]. Available: https://www.copenhagensubsea.com/ [Accessed Jun. 04, 2020].

[54] "Lian - Underwater thrusters." [Online]. Available: http://lianinno.com/underwater-thrusters/ [Accessed Jun. 03, 2020].

[55] "Innerspace Corporation - Electric thrusters." [Online]. Available: https://innerspacethrusters.com/products/electric/model-1002-series/ [Accessed Jun. 08, 2020].

[56] Budynas-Nisbett, *Mechanical Engineering : Shigley's Mechanical Engineering Design*. McGraw-Hill, 8th editio ed., 2006.

[57] J. Simões Morais, *Desenho Técnico Básico - 3. Desenho de Construções Mecânicas*. Porto Editora, 2015.

[58] C. Venner and A. Lubrecht, *Tribology Series - Experimental Methods in Tribology*. Elsevier Science, 2000.

[59] J. He and Z.-F. Fu, *Modal Analysis*. Butterworth-Heinemann, 2001.

[60] J. Martinez Farfan, *Modal analysis of deepwater morring lines based on a variational formulation*. PhD thesis, Texas A&M University, 2013.